

# Origin of dissipative Fermi arc transport in Weyl semimetals

E. V. Gorbar,<sup>1,2</sup> V. A. Miransky,<sup>3</sup> I. A. Shovkovy,<sup>4</sup> and P. O. Sukhachov<sup>1</sup>

<sup>1</sup>*Department of Physics, Taras Shevchenko National Kiev University, Kiev, 03680, Ukraine*

<sup>2</sup>*Bogolyubov Institute for Theoretical Physics, Kiev, 03680, Ukraine*

<sup>3</sup>*Department of Applied Mathematics, Western University, London, Ontario N6A 5B7, Canada*

<sup>4</sup>*College of Letters and Sciences, Arizona State University, Mesa, Arizona 85212, USA*

(Dated: December 3, 2024)

By making use of a low-energy effective model of Weyl semimetals, we show that the Fermi arc transport is dissipative. The origin of the dissipation is the scattering of the surface Fermi arc states into the bulk of the semimetal. It is noticeable that corresponding scattering rate is nonzero and can be estimated even in a perturbative theory, although in general the reliable calculations of transport properties necessitate a nonperturbative approach. Nondecoupling of the surface and bulk sectors in the low-energy theory of Weyl semimetals invalidates the usual argument of a nondissipative transport due to one-dimensional arc states. This property of Weyl semimetals is in drastic contrast to that of topological insulators, where the decoupling is protected by a gap in the bulk. Within the framework of the linear response theory, we obtain an approximate result for the conductivity due to the Fermi arc states and analyze its dependence on chemical potential, temperature, and other parameters of the model.

PACS numbers: 72.10.-d, 73.20.At, 73.25.+i, 71.10.-w

## I. INTRODUCTION

Dirac and Weyl semimetals, whose low-energy quasiparticle excitations are described by the Dirac and Weyl equations, respectively, became an active and vibrant area of research in condensed matter physics. Theoretically, Dirac semimetals were predicted to be realized in  $A_3\text{Bi}$  ( $A = \text{Na}, \text{K}, \text{Rb}$ ) and  $\text{Cd}_3\text{As}_2$  compounds [1, 2]. By using angle-resolved photoemission spectroscopy (ARPES), the Dirac nature of quasiparticles in the corresponding materials was indeed confirmed in Refs. [3–5], opening the path toward experimental investigations of the three-dimensional Dirac semimetals.

In momentum space, a Dirac point can be viewed as a superposition of two Weyl nodes of opposite chirality. If these nodes are separated in momentum or energy, then a Weyl semimetal is realized. Theoretically, the existence of Weyl semimetals was first predicted in pyrochlore iridates in Ref. [6]. Most recently, Weyl semimetals were experimentally discovered in Refs. [7–12], where the observations of characteristic surface Fermi arc states and unusual transport properties were reported for such compounds as TaAs, TaP, NbAs, NbP,  $\text{Mo}_x\text{W}_{1-x}\text{Te}$ , and  $\text{YbMnBi}_2$ .

One of the key features of both Dirac and Weyl semimetals is their unusual magnetotransport, which is profoundly affected by the chiral anomaly. The corresponding anomaly was originally discovered in high-energy physics in the analysis of the linearly divergent triangle diagrams [13]. It appears to have a qualitative effect also on magnetotransport of chiral plasmas [14]. As was first shown by Nielsen and Ninomiya [15], the longitudinal (with respect to the direction of the external magnetic field) magnetoresistivity in Weyl semimetals decreases with the growth of the magnetic field (called a negative magnetoresistivity phenomenon in the literature). This phenomenon was first observed experimentally in  $\text{Bi}_{1-x}\text{Sb}_x$  alloy with  $x \approx 0.03$  [16].

The physical reason for the negative magnetoresistivity is quite transparent [15, 17]. Since the lowest Landau level (LLL) states around each Weyl node are described by an effective one-dimensional chiral theory, they cannot backscatter on impurities. Therefore, the conductivity of such states is finite only due to backscattering between Weyl nodes with opposite chirality. Then, since the LLL density of states grows linearly with a magnetic field, the conductivity increases too. When the LLL contribution dominates, the total magnetoresistivity decreases with the field. We note, however, that theoretical analysis based on the Kubo's formula suggests that Dirac semimetals may also have a negative magnetoresistivity in the same regime [18]. Moreover, as argued in Ref. [19], the ionic impurity scattering can cause negative longitudinal magnetoresistivity in a generic three-dimensional metal in the quantum limit.

In fact, the absence of backscattering for one-dimensional chiral fermions provides the physical reason for the nondissipative electric transport in the quantum Hall effect (QHE) [20] resulting in a vanishing conductivity. It was shown in Ref. [21] that the fantastic exactness of the QHE conductivity is connected with nontrivial topological properties of QHE materials, which are encoded in the nonzero Chern numbers. Since the vacuum has trivial topological characteristics, current-carrying edge states are topologically protected that leads to the celebrated bulk-boundary correspondence.

The Haldane model [22] showed that the presence of an external magnetic field is not a necessary ingredient for the realization of the QHE. In fact, the first experimentally discovered two-dimensional topological insulator HgTe [23] can be considered as a combination of two copies of the Haldane model. Its nontrivial topological properties are described by the  $\mathbb{Z}_2$  index [24] and its conducting edge states are composed of two counterpropagating one-dimensional chiral fermions, related to each other through the time reversal transformation. In the absence of magnetic impurities, the edge states of a two-dimensional topological insulator are immune to backscattering and, thus, lead to a nondissipative transport.

A Weyl node also possesses nontrivial topological properties. It represents a monopole of the Berry curvature in momentum space, whose charge is connected with the chirality of the node. This is reflected in the characteristic properties of Weyl semimetals. One of them is the existence of the surface Fermi arc states, which are open segments of the Fermi surface connecting projections of the bulk cones onto the surface [6, 25, 26]. Such states connect the Fermi surfaces for the opposite chirality quasiparticles that otherwise would appear to be disconnected [26]. Experimentally, the Fermi arcs are directly observed with the help of the ARPES technique [8, 9].

Recently, the surface Fermi arcs were studied via another powerful technique, scanning tunneling spectroscopy (STS) [27, 28]. Theoretical calculations [29–31] and experimental studies [32–34] of quasiparticle interference (QPI) patterns caused by surface impurities or defects provide an alternative way to investigate surface Fermi arcs. Note that these QPI patterns are momentum space counterparts of Friedel oscillations [35]. Furthermore, the QPI reveals possible surface scattering processes, which cannot be directly measured by ARPES. However, the interpretation of QPI patterns strongly relies on theoretical calculations, providing a powerful, although indirect, evidence of Fermi arcs.

It is interesting that Dirac semimetals  $A_3\text{Bi}$  ( $A = \text{Na, K, Rb}$ ) also have Fermi arcs. It was shown in Ref. [36] that there exists a hidden “up-down” (*ud*) parity symmetry in the low-energy effective Hamiltonian that allows one to split the electron states into two separate sectors, with each describing a Weyl semimetal. Therefore, the corresponding Dirac semimetals are, in fact,  $\mathbb{Z}_2$  Weyl semimetals.

As suggested in Ref. [37], the surface Fermi arc states can be detected indirectly by measuring the density of states in surface-sensitive probes. Indeed, when a magnetic field is applied to a Weyl semimetal, a special type of closed magnetic orbits, involving both the surface Fermi arcs and the bulk states, are predicted to exist [37]. The corresponding orbits produce periodic quantum oscillations of the density of states with a characteristic dependence on the separation between the Weyl nodes in momentum space (transport experiments which probe the electronic properties of these orbits were suggested in Ref. [38]). The corresponding quantum oscillations were recently experimentally observed [39] in the Dirac semimetal  $\text{Cd}_3\text{As}_2$ . As was shown in Ref. [40], these quantum oscillations also encode the effects of interaction, which are predicted to modify the length of the Fermi arcs. In particular, one expects to see a nontrivial dependence of the quantum oscillations on the orientation of the magnetic field projection in the plane of the semimetal surface [40]. By numerically studying a minimal model of a Weyl semimetal, it was recently shown in Ref. [41] that the area enclosed by the Fermi surface and quantum oscillations in the thin film limit strongly depend on the in-plane magnetic field component parallel to the Weyl nodes splitting even in the non-interacting free theory.

Since the Fermi arcs in Weyl semimetals are topologically protected, it is natural that they are described by an effective Hamiltonian of one-dimensional chiral fermions. This suggests that the electron transport via Fermi arcs should be nondissipative. The latter would be a rather rigorous conclusion if the effective one-dimensional Hamiltonian of arc states stayed generally intact in the presence of impurities and disorder. However, as will be argued in this work, the situation is more complicated, and this is not necessarily the case. Indeed, as was shown in Ref. [42], in materials without a gap, “surface” quasiparticles are dephased by coupling to the bulk. It was argued in Ref. [31] that in such a case there is no simple effective theory for surface states because the surface Green’s functions for a Weyl semimetal necessarily contain the information about the electronic propagation from the surface into the bulk and back to the surface.

The paper is organized as follows. The effective Hamiltonian of the surface Fermi arc states in the simplest model of Weyl semimetal and a model of disorder used in the present paper are described in Sec. II. The Fermi arc conductivity in the effective one-dimensional surface model is considered both in naive and nonperturbative approaches in Sec. III. Perturbative signs of dissipation in the full model are revealed and analyzed in Sec. IV. The quasiparticle width and Fermi arc conductivity in the full model are calculated in Sec. V. The obtained results are discussed and summarized in Sec. VI.

For convenience, throughout the paper, we set  $\hbar = 1$ .

## II. MODEL OF A WEYL SEMIMETAL AND FERMI ARC STATES

In order to present our arguments as simple as possible, in this paper we study one of the simplest continuum models of a Weyl semimetal proposed by Okugawa and Murakami [43]. The Hamiltonian of the model describes a

pair of Weyl nodes separated in momentum space

$$H(\mathbf{k}) = \gamma (k_z^2 - m) \sigma_z + v_F (k_x \sigma_x + k_y \sigma_y), \quad (1)$$

where  $v_F$ ,  $m$  and  $\gamma$  are positive constants. As is easy to check, the two Weyl nodes are located at  $k_z = \pm\sqrt{m}$ . We assume that, in coordinate space, the semimetal is in the upper half-plane  $y > 0$  and the vacuum is in the lower half-plane  $y < 0$ . In order to prevent quasiparticles from escaping into the vacuum region, we set  $m \rightarrow -\tilde{m}$  and take the limit  $\tilde{m} \rightarrow \infty$  for  $y < 0$ . Because of the semimetal surface at  $y = 0$ , the translation invariance in the  $y$  direction is broken. Therefore, we keep the operator form for  $k_y = -i\partial_y$  in Hamiltonian (1).

By considering the eigenvalue problem  $H\psi = E\psi$ , it is not difficult to find the wave-functions of the surface states in semimetal and vacuum,

$$\psi_{y>0} = \sqrt{p(k_z)} e^{ik_x x + ik_z z - p(k_z)y} \begin{pmatrix} 1 \\ 1 \end{pmatrix}, \quad (2)$$

$$\psi_{y<0} = \sqrt{p(k_z)} e^{ik_x x + ik_z z + \gamma\tilde{m}y} \begin{pmatrix} 1 \\ 1 \end{pmatrix}, \quad (3)$$

respectively, where  $p(k_z) = \gamma(m - k_z^2)/v_F$  and  $-\sqrt{m} < k_z < \sqrt{m}$ . The corresponding expression for the surface state energy reads

$$E_s = v_F k_x. \quad (4)$$

The effective Hamiltonian for the surface Fermi arc states is given by (see Ref. [44] for a derivation of the effective Hamiltonian for the surface states in topological insulators)

$$H_{\text{surf}} = -iv_F \partial_x \quad (5)$$

and, as expected, describes one-dimensional chiral fermions.

The energy spectrum of model (1) is shown in Fig. 1. In order to obtain the corresponding numerical results, we chose the model parameters as in Ref. [1], i.e.,

$$m = 0.0082 \text{ \AA}^{-2}, \quad \gamma = 10.6424 \text{ eV \AA}^2, \quad v_F = 2.4598 \text{ eV \AA}, \quad a = 5.448 \text{ \AA}, \quad c = 9.655 \text{ \AA}. \quad (6)$$

This choice mimics the effective low-energy description of Na<sub>3</sub>Bi. As we see from Fig. 1, the Fermi surface consists of the bulk sheets connected by a Fermi arc.

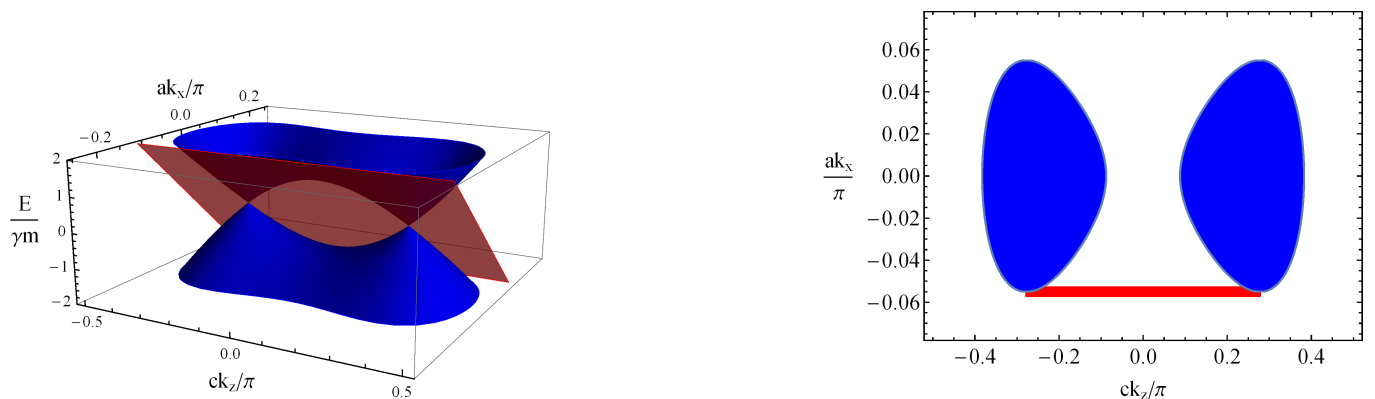


FIG. 1: (Color online) The bulk (blue) and Fermi arc (red) states in the model of Weyl semimetal at  $y > 0$  given by Eq. (1) (left panel). Its Fermi surface is plotted for the Fermi energy  $E_F/(\gamma m) = 0.9$  (right panel).

In our study of Fermi arcs transport, we will use the simplest model of quenched disorder, in which the interaction of electrons with impurities is described by the following Hamiltonian:

$$H_{\text{dis}} = \int d\mathbf{r} \psi^\dagger(\mathbf{r}) U(\mathbf{r}) \psi(\mathbf{r}) \quad (7)$$

with the local disorder potential

$$U(\mathbf{r}) = \sum_j u(\mathbf{r} - \mathbf{r}_j) = \sum_j u_0 \delta(\mathbf{r} - \mathbf{r}_j) \quad (8)$$

whose strength is determined by  $u_0$ . This simple form of disorder greatly simplifies many calculations. In some cases, however, the singular nature of the  $\delta$ -function may cause unphysical divergencies. When that happens, one may replace the potential in Eq. (8) with a Gaussian function, i.e.,

$$U(\mathbf{r}) = \sum_j u_0 \frac{e^{-\frac{(\mathbf{r}-\mathbf{r}_j)^2}{2g^2}}}{(2\pi g^2)^{3/2}}. \quad (9)$$

The translation invariance, which is broken by the disorder, can be effectively restored by averaging over the positions of impurities, i.e.,

$$\langle A(\mathbf{r}) \rangle_{\text{dis}} = \frac{1}{V} \sum_j \int d^3\mathbf{r}_j A(\mathbf{r}_j), \quad (10)$$

where  $V$  is the volume of the system. The impurity correlation function for the local disorder with the potential in Eq. (8) is

$$\langle u(\mathbf{r} - \mathbf{r}_j) u(\mathbf{r}' - \mathbf{r}_j) \rangle_{\text{dis}} = u_0^2 n_{\text{imp}} \delta(\mathbf{r} - \mathbf{r}'), \quad (11)$$

where  $n_{\text{imp}} = N_{\text{imp}}/V$  is the concentration of impurities.

### III. FERMI ARCS CONDUCTIVITY IN THE EFFECTIVE ONE-DIMENSIONAL MODEL

In this section, we investigate the transport properties of the surface Fermi arc states by using the effective one-dimensional model (5). The tacit assumption of such an approach is that the dynamics of the surface states decouples from the dynamics of the bulk states. (As we argue later, this is not the case in Weyl semimetals.)

We will utilize the Kubo's linear response formalism. Formally, the conductivity tensor is expressed through the retarded current-current correlation function, i.e.,

$$\sigma_{nm}(\omega; \mathbf{r}, \mathbf{r}') = -\frac{i}{\omega} \Pi_{nm}(\omega; \mathbf{r}, \mathbf{r}'), \quad (12)$$

where the correlator itself is defined via the following ground state expectation value:

$$\Pi_{nm}(t - t'; \mathbf{r}, \mathbf{r}') = i\theta(t - t') \langle [j^n(t, \mathbf{r}), j^m(t', \mathbf{r}')] \rangle. \quad (13)$$

To one-loop order, the correlation function is given by the following expression:

$$\Pi_{xx}(i\Omega_n; \mathbf{r}, \mathbf{r}') = e^2 v_F^2 T \sum_{i\omega_l} \langle G(i\omega_l; \mathbf{r}, \mathbf{r}') G(i\omega_l - i\Omega_n; \mathbf{r}', \mathbf{r}) \rangle_{\text{dis}}, \quad (14)$$

where  $\omega_l = (2l + 1)\pi T$  and  $\Omega_n = 2n\pi T$  are the fermion and boson Matsubara frequencies, respectively. As usual, the retarded forms of the correlation functions and propagators are obtained by replacing  $i\omega_l \rightarrow \omega + i0$  and  $i\Omega_n \rightarrow \Omega + i0$ . After averaging the expression in Eq. (14) over the positions of impurities, we obtain a translation invariant result  $\Pi(i\Omega_n; \mathbf{r} - \mathbf{r}')$ .

#### A. Approximation without cross-correlation diagrams

In order to derive an approximate result for the conductivity, one might try replacing the average  $\langle G(i\omega_l; \mathbf{r}, \mathbf{r}') G(i\omega_l - i\Omega_n; \mathbf{r}', \mathbf{r}) \rangle_{\text{dis}}$  with the product  $\langle G(i\omega_l; \mathbf{r}, \mathbf{r}') \rangle_{\text{dis}} \langle G(i\omega_l - i\Omega_n; \mathbf{r}', \mathbf{r}) \rangle_{\text{dis}}$  in the definition of the current-current correlator (14). In three-dimensional models, such an approximation is usually not too bad. However, as is well known and as we show below, it fails in the one-dimensional model at hand. Still, such an approximation is instructive for the later study of the full model as a useful reference point.

By taking into account that each disorder-averaged propagator is translation invariant, it is natural to use the momentum-space representation for the correlation function:

$$\Pi_{xx}(i\Omega_n, \mathbf{q}) \simeq e^2 v_F^2 T \sum_{i\omega_l} \int \frac{d\mathbf{k}}{(2\pi)^2} \langle G(i\omega_l, \mathbf{k}) \rangle_{\text{dis}} \langle G(i\omega_l - i\Omega_n, \mathbf{k} - \mathbf{q}) \rangle_{\text{dis}}, \quad (15)$$

where  $\langle G(i\omega_l; \mathbf{k}) \rangle_{\text{dis}}$  is the Fourier transform of the coordinate-space propagator averaged over the positions of impurities. Furthermore, it is convenient to express the propagator in terms of its spectral function  $A(\omega, \mathbf{k})$ ,

$$\langle G(i\omega_l, \mathbf{k}) \rangle_{\text{dis}} = \int_{-\infty}^{\infty} d\omega \frac{A(\omega, \mathbf{k})}{i\omega_l + \mu - \omega}, \quad (16)$$

where, by definition,

$$A(\omega, \mathbf{k}) = \frac{i}{2\pi} [\langle G^R(\omega, \mathbf{k}) \rangle_{\text{dis}} - \langle G^A(\omega, \mathbf{k}) \rangle_{\text{dis}}]_{\mu=0} = \frac{i}{2\pi} [\langle G(\omega + i0, \mathbf{k}) \rangle_{\text{dis}} - \langle G(\omega - i0, \mathbf{k}) \rangle_{\text{dis}}]_{\mu=0}. \quad (17)$$

In terms of the spectral function, the conductivity can be expressed as follows:

$$\sigma_{xx}(\Omega, \mathbf{q}) = -\frac{i}{\Omega} e^2 v_F^2 \int \frac{d\mathbf{k}}{(2\pi)^2} \int \int d\omega d\omega' \frac{n(\omega - \mu) - n(\omega' - \mu)}{\omega - \omega' - \Omega - i0} A(\omega, \mathbf{k}) A(\omega', \mathbf{k} - \mathbf{q}). \quad (18)$$

Note that, in the last expression, we calculated the sum over the Matsubara frequencies and performed the appropriate analytical continuation to real values of frequencies,  $i\Omega_n \rightarrow \Omega + i0$ .

The expression for the DC conductivity of the Fermi arcs can now be obtained from Eq. (18) by calculating the appropriate limit:  $q \rightarrow 0$  and  $\Omega \rightarrow 0$ . The correct order of limits is to take the long-range limit ( $q \rightarrow 0$ ) first and the static limit ( $\Omega \rightarrow 0$ ) second. Then, one derives the following general result for the real part of the DC conductivity:

$$\Re \sigma_{xx}(0, 0) = -\frac{e^2 v_F^2}{8T} \int \frac{d\mathbf{k}}{2\pi} \int d\omega \frac{A(\omega, \mathbf{k}) A(\omega, \mathbf{k})}{\cosh^2\left(\frac{\omega - \mu}{2T}\right)}, \quad (19)$$

where we used the Sokhotski formula in order to extract the real part.

## B. Simple model for the quasiparticle decay width

In the effective model (5), the explicit form of the free (causal) propagator for the Fermi arc states reads

$$G_{\text{arc}}(\omega, \mathbf{k}) = i \frac{\theta(m - k_z^2)}{\omega + \mu - v_F k_x + i0 \text{sign}(\omega)}. \quad (20)$$

Notice the overall factor  $\theta(m - k_z^2)$ , which takes into account the fact that the arc states exist only for a finite range of  $k_z$ :  $-\sqrt{m} < k_z < \sqrt{m}$ . The spectral function of the corresponding surface propagator is obtained by making use of the definition in Eq. (17),

$$A(\omega, \mathbf{k}) = i\delta(\omega - v_F k_x) \theta(m - k_z^2). \quad (21)$$

As is clear, this model describes surface Fermi arc quasiparticles with a vanishing decay width. A nonzero decay width  $\Gamma$  can be introduced semi-rigorously by replacing the  $\delta$ -function in the last expression with a Lorentzian distribution,

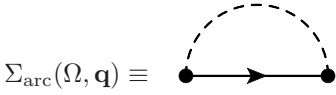
$$A_{\Gamma}(\omega, \mathbf{k}) = \frac{i}{\pi} \frac{\Gamma}{(\omega - v_F k_x)^2 + \Gamma^2} \theta(m - k_z^2). \quad (22)$$

As we will argue later, it is indeed justified to introduce a nonzero decay width for the Fermi arc quasiparticles. Here we will ignore the fact that the specific model details in Eq. (22) may not capture all realistic properties of surface quasiparticles.

In order to make a rough estimate for the quasiparticle width of the Fermi arc states, we can use a perturbation theory in the impurity potential. In the model of quenched disorder with a local potential, the impurity correlation function (11) in momentum space is given by

$$D(\omega, \mathbf{k}) = n_{\text{imp}} u_0^2 (2\pi) \delta(\omega). \quad (23)$$

Then, to one-loop order, the electron self-energy of the surface Fermi arcs states equals



$$\Sigma_{\text{arc}}(\Omega, \mathbf{q}) \equiv \text{---} \bullet \xrightarrow{\hspace{1cm}} \bullet \text{---} = -i \int \frac{d\omega d^2\mathbf{k}}{(2\pi)^3} G_{\text{arc}}(\omega, \mathbf{k}) D(\Omega - \omega, \mathbf{q} - \mathbf{k}) = -in_{\text{imp}} u_0^2 \int \frac{d^2\mathbf{k}}{(2\pi)^2} G_{\text{arc}}(\Omega, \mathbf{k}). \quad (24)$$

By making use of Eq. (20), we find

$$\Sigma_{\text{arc}}(\omega, 0) = -in_{\text{imp}} u_0^2 \frac{\sqrt{m}}{2\pi v_F}. \quad (25)$$

Thus, in this approximation, the quasiparticle width is given by

$$\Gamma = n_{\text{imp}} u_0^2 \frac{\sqrt{m}}{2\pi v_F}. \quad (26)$$

Finally, by making use of the general result for the DC conductivity in Eq. (19), we derive

$$\Re \sigma_{xx}(0, 0) = \frac{e^2 v_F^2}{8T\pi^2} \frac{\sqrt{m}}{\pi} \int dk_x \int d\omega \frac{1}{\cosh^2\left(\frac{\omega - \mu}{2T}\right)} \frac{\Gamma^2}{[(\omega - v_F k_x)^2 + \Gamma^2]^2} = \frac{e^2 v_F \sqrt{m}}{4\Gamma\pi^2}. \quad (27)$$

Formally, this result for the conductivity shows that the transport is Ohmic (dissipative) whenever the surface arc quasiparticles have a nonzero width. The nondissipative regime is possible only when the quasiparticle width vanishes, i.e.,  $\Gamma \rightarrow 0$ . Therefore, the issue of the quasiparticle width for the surface states appears to be an important aspect that can shed light on the nature of the arc's transport. We will try to resolve this issue later. Before doing that, however, we should also address the validity of the approximation for the current-current correlator with cross-correlation diagrams neglected. As is well known and as we show below, such an approximation is not reliable. It will be essential, therefore, to account for some cross-correlations. This will be done via the inclusion of the appropriate vertex corrections in Sec. VB.

### C. Nondissipative transport from nonperturbative treatment in one-dimensional

It is easy to show that the naive calculation of the conductivity in the previous subsection is unreliable for one-dimensional chiral fermions, described by the effective low-energy model (5). The corresponding argument is well known [45].

In the presence of quenched disorder in one-dimension, the eigenstate wave-functions for chiral fermions can be calculated exactly (note the absence of backscattering)

$$\psi_E(x) = e^{\frac{i}{v_F} [Ex - \sum_j u_0 \int_{x_0}^x dz \delta(z - x_j)]}, \quad (28)$$

leading to the following exact Green's function for the corresponding Fermi arcs states:

$$G(\omega; x, x') = i \int \frac{dE}{2\pi} \frac{1}{\omega + \mu - E} e^{\frac{i}{v_F} [E(x - x') - \sum_j u_0 (\theta(x - x_j) - \theta(x' - x_j))]} \quad (29)$$

As we see from this nonperturbative result, the disorder potential appears only as a single phase  $\sum_j u_0 [\theta(x - x_j) - \theta(x' - x_j)]$  in the exponent. Moreover, the phase is such that it changes the overall sign under the interchange of  $x$  and  $x'$ . Therefore, after substituting propagator (29) into the expression for the retarded current-current correlation function (14), we find that all effects of disorder drop out from the final result. In other words, in the effective one-dimensional surface model defined by Eq. (5), disorder does not affect the Fermi arc transport, i.e., the transport is nondissipative. One should note, however, that this conclusion does not necessarily imply the vanishing quasiparticle width for the surface states. The corresponding width  $\Gamma$  is a characteristic of the propagator (29) averaged over the disorder. Irrespective of the actual value of such a width, it does not affect the result for the correlation function (14). This is in contrast to the naive arguments of Sec. IIIB, which relied on the approximation where the cross-correlation between the quasiparticle propagators was neglected. This simple observation is instructive and should be kept in mind in the analysis of transport properties of the Fermi arc states in a more realistic model of a Weyl (semi-)metal in the next section.

#### IV. PERTURBATIVE SIGNS OF DISSIPATION IN THE FULL MODEL

As we showed in the previous section, the absence of dissipation in the Fermi arc transport in the one-dimensional effective model of chiral fermions is connected with its very unique property that all effects of quenched disorder in the exact Green's function  $G(\omega; x, x')$  are captured in a single phase factor, which is odd under the interchange of  $x$  and  $x'$ . Because of its special property, the phase factor drops out of the expression for the current-current correlator, i.e., disorder has no effect on the transport.

Below, we will argue that the full effective model of Weyl semimetals (1), which necessarily contains both the surface Fermi arc states and the bulk states, does not share this property. The formal reasons for this are (i) the loss of one-dimensional kinematic constraint in scattering of chiral fermions and (ii) the nondecoupling of the low-energy dynamics of the two types of states (i.e., surface and bulk). From a physical viewpoint, this immediately leads to a dissipation because the surface Fermi arc states can easily scatter into the bulk. With the loss of exact integrability in the full model, of course, we cannot present an exact solution supporting this claim. Instead, we will use physical arguments that strongly support nondecoupling and dissipation.

Let us consider the scattering of the Fermi arc states using the Born approximation. A convenient starting point for such an analysis is the Lippmann–Schwinger equation for the surface states,

$$\psi_s(\mathbf{r}) = \psi_s^{(0)}(\mathbf{r}) - i \int d^3\mathbf{r}' S(\mathbf{r}, \mathbf{r}') U(\mathbf{r}') \psi_s(\mathbf{r}'), \quad (30)$$

where  $\psi_s^{(0)}(\mathbf{r}) \equiv \psi_{y>0}$  is the incident surface wave as in Eq. (2). Strictly speaking, here we should use a regularized Gaussian form of the disorder potential  $U(\mathbf{r}')$ , given in Eq. (9). Indeed, if a point-like interaction is used, the second term in the Lippmann–Schwinger equation would give a contribution to the wave-function  $\sum_j u_0 S(\mathbf{r}, \mathbf{r}_j) \psi_s(\mathbf{r}_j)$ , which diverges at the location of impurities.

In general, solving the Lippmann–Schwinger equation is a quite difficult (nonperturbative) problem. Instead, here we will consider a perturbative solution in the Born approximation, in which the surface state wave-function on the right hand side of Eq. (30) is replaced with  $\psi_s^{(0)}(\mathbf{r})$ .

It may be instructive to recall that the Born approximation can be readily derived from the spectral problem,  $(H_0 + U)\psi = E\psi$ . Assuming a perturbative expansion of the solution in the form  $\psi \simeq \psi^{(0)} + \psi^{(1)}$ , where  $\psi^{(0)}$  are the eigenstates of the free Hamiltonian  $H_0$ , we easily derive the formal result for the first order correction:  $\psi^{(1)} = (E - H_0)^{-1} U \psi^{(0)}$ . Noting that  $S \equiv i(E - H_0)^{-1}$  is the operator form of the free propagator and taking into account its coordinate-space representation, we see that  $\psi^{(1)}$  coincides with the second term in Eq. (30) in the Born approximation.

##### A. Free propagator in the full model

In the clean limit (i.e., no disorder), it is straightforward to derive an explicit expression for the retarded quasiparticle Green's function (free propagator) in the full effective model (1) by making use of the general definition:  $S^R(\omega, \mathbf{r}, \mathbf{r}') \equiv i \sum_E \psi_E(\mathbf{r}) \psi_E^\dagger(\mathbf{r}') / (\omega - E + i0)$ , where the sum runs over a complete set of the energy eigenstates. By taking into account that the Hilbert space of the corresponding eigenvalue problem contains both bulk and surface states, the resulting Green's function naturally splits into the surface and bulk contributions:

$$S^R(\omega, \mathbf{r}, \mathbf{r}') = \int \frac{d^2\mathbf{k}_\parallel e^{i\mathbf{k}_\parallel(\mathbf{r}_\parallel - \mathbf{r}'_\parallel)}}{(2\pi)^2} S_s^R(\omega, \mathbf{k}_\parallel; y, y') + \int \frac{d^3\mathbf{k} e^{i\mathbf{k}(\mathbf{r} - \mathbf{r}')}}{(2\pi)^3} S_b^R(\omega, \mathbf{k}). \quad (31)$$

In the model at hand, the explicit forms of the two types of the Green's functions are

$$S_s^R(\omega, \mathbf{k}_\parallel; y, y') = ip(k_z) \frac{(1 + \sigma_x) e^{-(y+y')p(k_z)}}{\omega - v_F k_x + i0}, \quad (32)$$

$$S_b^R(\omega, \mathbf{k}) = i \frac{\omega + \gamma(k_z^2 - m)\sigma_z + v_F(k_x \sigma_x + k_y \sigma_y)}{\omega^2 - E(k)^2 + i0 \text{sign}(\omega)}, \quad (33)$$

where  $E(k) = \pm \sqrt{\gamma^2(k_z^2 - m)^2 + v_F^2(k_x^2 + k_y^2)}$ . [Strictly speaking, the Green's function of bulk states is not translation invariant in the presence of the surface at  $y = 0$ . However, this is relevant only near the surface and we checked that taking into account the translation non-invariance of the bulk Green's function does not affect our qualitative

conclusions. Therefore, for the sake of simplicity, we use the translation invariant Green's function of the bulk states.] Note that the coordinate-space representation of the surface Green's function of the Fermi arc states is given by

$$S_s^R(\omega; \mathbf{r}, \mathbf{r}') = \frac{\theta(x-x') e^{\frac{i\omega(x-x')}{v_F}}}{2\pi v_F} (1 + \sigma_x) F_{\mathbf{r}, \mathbf{r}'}, \quad (34)$$

where

$$F_{\mathbf{r}, \mathbf{r}'} = \frac{1}{8\sqrt{v_F}\gamma^{3/2}(y+y')^{5/2}} \left\{ -4\sqrt{\gamma v_F(y+y')} [v_F(z-z') \sin(\sqrt{m}(z-z')) + 2\gamma\sqrt{m}(y+y') \cos(\sqrt{m}(z-z'))] \right. \\ \left. + i\sqrt{\pi} e^{\frac{v_F(z-z')^2}{4\gamma(y+y')} - \frac{\gamma m(y+y')}{v_F}} \left[ \text{Erf} \left( \frac{v_F(z-z') - 2i\sqrt{m}\gamma(y+y')}{2\sqrt{v_F}\gamma(y+y')} \right) - \text{Erf} \left( \frac{v_F(z-z') + 2i\sqrt{m}\gamma(y+y')}{2\sqrt{v_F}\gamma(y+y')} \right) \right] \right. \\ \left. \times [v_F^2(z-z')^2 + 2v_F\gamma(y+y') + 4m\gamma^2(y+y')^2] \right\}, \quad (35)$$

and  $\text{Erf}(z) = \frac{2}{\sqrt{\pi}} \int_0^z e^{-t^2} dt$  is the error function [46]. By making use of the well-known asymptotic behavior of the error function (see formula 7.1.23 in Ref. [46]), we derive the following results:

$$F_{\mathbf{r}, \mathbf{r}'} \simeq -4\sqrt{m}\gamma \frac{\cos(\sqrt{m}(z-z'))}{v_F(z-z')^2} + \mathcal{O}\left(\frac{1}{(z-z')^3}\right), \quad \text{for } z \rightarrow \infty, \quad (36)$$

$$F_{\mathbf{r}, \mathbf{r}'} \simeq \frac{v_F \cos(\sqrt{m}(z-z'))}{\sqrt{m}\gamma(y+y')^2} + \mathcal{O}\left(\frac{1}{(y+y')^3}\right), \quad \text{for } y \rightarrow \infty. \quad (37)$$

Interestingly, we find that  $F_{\mathbf{r}, \mathbf{r}'}$  falls off as a power-law function of  $y$ , rather than an exponential function, when  $y \rightarrow \infty$ . At first sight, this seems surprising since (almost) all surface states, see Eq. (2), have an exponential dependence on  $y$ . The puzzle is resolved by noting that the exponents vanish near the ends of the Fermi arcs, i.e., when  $k_z \rightarrow \pm\sqrt{m}$ . Thus, when integrating over all momenta in the surface Green's function, the contributions from the regions with a (nearly) vanishing exponent dominate the coordinate-space asymptotes. In fact, this is also an indication that the dynamics of the surface arc states in the full model does not decouple from the dynamics of the bulk states.

## B. Scattering of Fermi arc states in the Born approximation

By making use of the general result in the Born approximation and the explicit form of the free propagator (31), to the first order in the disorder potential, the scattered wave is given by

$$\psi^{(1)}(\mathbf{r}) = \psi_s^{(1)}(\mathbf{r}) + \psi_b^{(1)}(\mathbf{r}), \quad (38)$$

$$\psi_s^{(1)}(\mathbf{r}) \simeq -i \int d^3\mathbf{r}' S_s^R(\mathbf{r}, \mathbf{r}') U(\mathbf{r}') \psi_s^{(0)}(\mathbf{r}') \simeq -iu_0 \sum_j S_s^R(\mathbf{r}, \mathbf{r}_j) \psi_s^{(0)}(\mathbf{r}_j), \quad (39)$$

$$\psi_b^{(1)}(\mathbf{r}) \simeq -i \int d^3\mathbf{r}' S_b^R(\mathbf{r}, \mathbf{r}') U(\mathbf{r}') \psi_s^{(0)}(\mathbf{r}') \simeq -iu_0 \sum_j S_b^R(\mathbf{r}, \mathbf{r}_j) \psi_s^{(0)}(\mathbf{r}_j). \quad (40)$$

Note that there are separate surface and bulk waves. This is in agreement with the structure of the quasiparticle Green's function in the full model, which contains both the surface and bulk contributions, see Eqs. (31) through (33). As mentioned earlier, a regularized version of the impurity potential (9) should be used in the above expression for the scattered bulk wave. Otherwise, the result will be singular at  $\mathbf{r} \rightarrow \mathbf{r}_j$ . For the purposes of extracting the outgoing waves at large distances  $r \rightarrow \infty$ , however, it suffices to use the local form of the potential given by Eq. (8).

Then, by making use of the propagator in Eq. (32) and the  $z \rightarrow \infty$  asymptote from Eq. (36), we derive the following result for the surface part of the scattered wave:

$$\psi_s^{(1)}(\mathbf{r}) \simeq 4i\sqrt{m}\gamma u_0 \sum_j \frac{\theta(x-x_j) \cos[\sqrt{m}(z-z_j)]}{\pi v_F^2(z-z_j)^2} \sqrt{p(k_z)} e^{ik_x x + ik_z z_j - p(k_z) y_j} \begin{pmatrix} 1 \\ 1 \end{pmatrix}. \quad (41)$$

While the  $x$ -component of momentum  $k_x$  remains unchanged in the scattered wave, the  $z$ -component of momentum drastically changes from the original value  $k_z$ , constrained only by its range:  $-\sqrt{m} < k_z < \sqrt{m}$ . Indeed, the outgoing

wave is a superposition of two waves with limiting values of the momenta,  $k_z = \pm\sqrt{m}$ . Since the distinction between the two types of states fades away in the corresponding region of the phase space, one might argue that the Fermi arc states are pushed towards the bulk states.

In the case of a single impurity, the representative numerical results for the scattered surface portion of the wavefunction,  $\psi_s^{(1)}$ , are shown in Fig. 2. As one can see from the  $x$ -dependence in the left panel, there is no backscattering (i.e., into the region  $x < 0$ ) of the surface wave. In the region  $x > 0$ , the  $\pi/2$  phase shift between the real and imaginary parts of  $\psi_s^{(1)}$  suggests a characteristic behavior,  $e^{ik_x x}$ , of a plane wave propagating forward. The other two panels in Fig. 2 show the profiles of the real and imaginary parts of the scattered wave in the  $y$  direction (into the bulk) and the  $z$  direction (along the surface). These latter two are of no particular significance by themselves. However, they will serve as a useful benchmark later in our comparison with the waves scattered into the bulk.

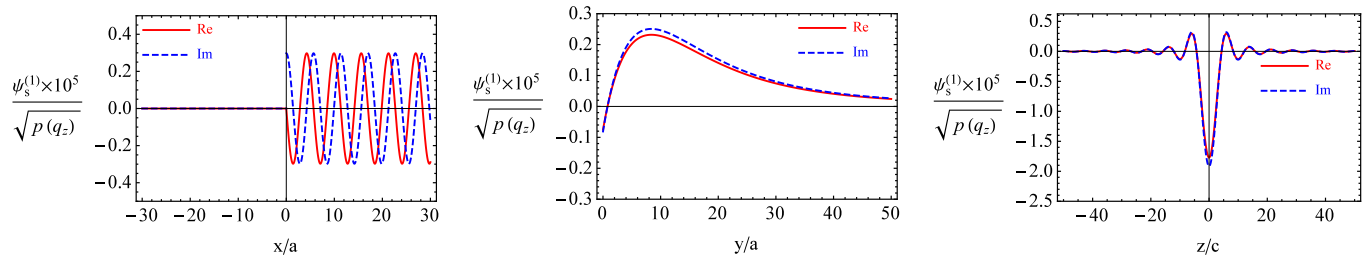


FIG. 2: (Color online) The upper component of the surface part of scattered wave  $\psi_s^{(1)}$ , defined by Eq. (41), as a function of  $x/a$  (left panel),  $y/a$  (middle panel), and  $z/c$  (right panel). The numerical values of the model parameters are  $u_0 = 0.1$  eV  $\text{\AA}^3$ ,  $\omega = 0.5$  eV,  $\mathbf{q} = (0, 0, 0)$ ,  $\mathbf{r}_j = (\omega/v_F, 0, 0)$ , and  $a$  and  $c$  are defined in Eq. (6). The wave function is shown for  $\mathbf{r} = (x, 5a, 5c)$  in the left panel,  $\mathbf{r} = (5a, y, 5c)$  in the middle panel, and  $\mathbf{r} = (5a, 5a, z)$  in the right panel.

In order to calculate the bulk part of the scattered wave (40), we use the bulk propagator (33) in momentum space and derive

$$\psi_b^{(1)}(\mathbf{r}) = u_0 \sum_j \int \frac{d^3\mathbf{k}}{(2\pi)^3} \frac{e^{i\mathbf{k}(\mathbf{r}-\mathbf{r}_j)}}{\omega^2 - E(k)^2 + i0 \text{sign}(\omega)} [\omega + \gamma(k_z^2 - m)\sigma_z + v_F(k_x\sigma_x + k_y\sigma_y)] \psi_s^{(0)}(\mathbf{r}_j). \quad (42)$$

In this expression, two out of three momentum integrations can be performed analytically. Then, the result reads

$$\begin{aligned} \psi_b^{(1)}(\mathbf{r}) = & -u_0 \sum_j \int \frac{dk_z}{4\pi^2 v_F^2} e^{ik_z(z-z_j)} \left\{ [\omega + \gamma(k_z^2 - m)\sigma_z] \left[ \theta(-\Omega^2) K_0 \left( \frac{\rho|\Omega|}{v_F} \right) + i\frac{\pi}{2} \theta(\Omega^2) H_0^{(1)} \left( \text{sign}(\omega) \frac{\rho|\Omega|}{v_F} \right) \right] \right. \\ & \left. + i\frac{|\Omega|}{\rho} [(x-x_j)\sigma_x + (y-y_j)\sigma_y] \left[ \theta(-\Omega^2) K_1 \left( \frac{\rho|\Omega|}{v_F} \right) + i\text{sign}(\omega) \frac{\pi}{2} \theta(\Omega^2) H_1^{(1)} \left( \text{sign}(\omega) \frac{\rho|\Omega|}{v_F} \right) \right] \right\} \psi_s^{(0)}(\mathbf{r}_j), \end{aligned} \quad (43)$$

where, by definition,  $\Omega^2 \equiv \omega^2 - \gamma^2(k_z^2 - m)^2$  and  $\rho^2 \equiv (x-x_j)^2 + (y-y_j)^2$ .

In the case of a single impurity, the numerical results for the scattered bulk portion of the wavefunction,  $\psi_b^{(1)}$ , are shown in Figs. 3 and 4. From the  $x$ -dependence of the scattered wave, presented in the left panels of Figs. 3 and 4, we see clearly that backscattering is present. This is in contrast to the surface scattered wave, studied earlier. There are also qualitative differences in the  $z$  and  $y$  dependence of the scattered bulk wave, presented in the middle and right panels of Figs. 3 and 4, respectively. Unlike the corresponding surface counterparts, studied earlier, these results reveal outgoing waves propagating into the bulk. This is suggested by the characteristic phase shift of  $\pi/2$  between the real and imaginary parts of all components of the wavefunction.

It is interesting to study the asymptotes of the bulk scattered wave  $\psi_b^{(1)}(\mathbf{r})$  at large values of the coordinates along the surface of the semimetal, i.e.,  $x \gg a$  and  $z \gg a$ . Both asymptotes reveal a long-range (propagating) tail with a weak modulation of the amplitudes. This is demonstrated in Fig. 5, in which we show the real part of the upper component of  $\psi_b^{(1)}$  as a function of  $x/a$  (left panel) and as a function of  $z/c$  for large values of the arguments. Note, that the red shaded area in the plot is an outcome of many oscillations with a small period. From the numerical result in Fig. 5, we find that the amplitude of the large scale modulations decreases as  $1/x$  at large  $x/a$  and as  $1/z^2$  at large  $z/c$ . As one can check, the same qualitative behavior is valid for the real part of the lower component of  $\psi_b^{(1)}$ , as well as for the imaginary parts of both components.

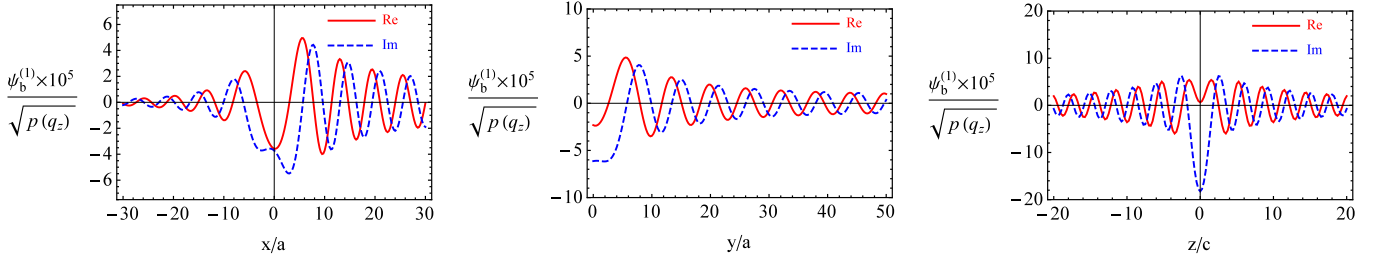


FIG. 3: (Color online) The upper component of the bulk part of scattered wave  $\psi_b^{(1)}$ , given by Eq. (43), as a function of  $x/a$  (left panel),  $y/a$  (middle panel), and  $z/c$  (right panel). The numerical values of the model parameters are  $u_0 = 0.1 \text{ eV } \text{\AA}^3$ ,  $\omega = 0.5 \text{ eV}$ ,  $\mathbf{q} = (\omega/v_F, 0, 0)$ ,  $\mathbf{r}_j = (0, 0, 0)$ . The wave function is shown for  $\mathbf{r} = (x, 5a, 5c)$  in the left panel,  $\mathbf{r} = (5a, y, 5c)$  in the middle panel, and  $\mathbf{r} = (5a, 5a, z)$  in the right panel.

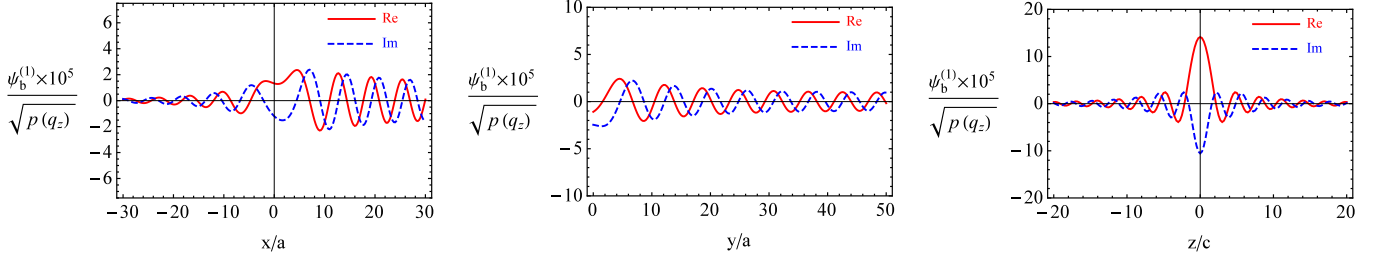


FIG. 4: (Color online) The lower component of the bulk part of scattered wave  $\psi_b^{(1)}$ , given by Eq. (43), as a function of  $x/a$  (left panel),  $y/a$  (middle panel), and  $z/c$  (right panel). The numerical values of the model parameters are  $u_0 = 0.1 \text{ eV } \text{\AA}^3$ ,  $\omega = 0.5 \text{ eV}$ ,  $\mathbf{q} = (\omega/v_F, 0, 0)$ ,  $\mathbf{r}_j = (0, 0, 0)$ . The wave function is shown for  $\mathbf{r} = (x, 5a, 5c)$  in the left panel,  $\mathbf{r} = (5a, y, 5c)$  in the middle panel, and  $\mathbf{r} = (5a, 5a, z)$  in the right panel.

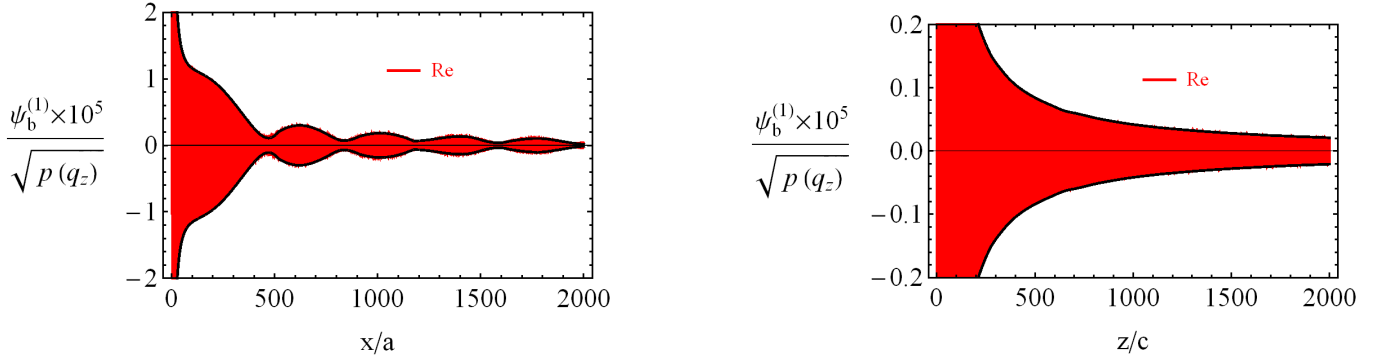


FIG. 5: (Color online) The real part of the upper component of the bulk part of scattered wave  $\psi_b^{(1)}$ , given by Eq. (43), as a function of  $x/a$  (left panel) and as a function of  $z/c$  for large values of arguments. The numerical values of the model parameters are  $u_0 = 0.1 \text{ eV } \text{\AA}^3$ ,  $\omega = 0.5 \text{ eV}$ ,  $\mathbf{q} = (\omega/v_F, 0, 0)$ ,  $\mathbf{r}_j = (0, 0, 0)$ . For plotting the results, we used  $\mathbf{r} = (x, 5a, 5c)$  in the left panel and  $\mathbf{r} = (5a, 5a, z)$  in the right panel.

To summarize our results, we find that, after scattering on an impurity, a surface wave produces not only (forward-scattered) surface states, but also waves propagating into the bulk. This implies that a naive low-energy consideration of the surface Fermi arc states is invalid. Indeed, such approximately one-dimensional states are not decoupled from the three-dimensional bulk states. In the context of transport properties, this means that a proper analysis of the dynamics with a mixing of the two types of states is required. This problem is addressed in the next section.

## V. FERMI ARC WIDTH AND CONDUCTIVITY IN THE FULL MODEL

In this section, we study the transport properties of the Fermi arcs in the full model (1) that contains not only the surface states, but also the gapless bulk states. As expected, the exact integrability of the full model is lost and we have to rely on some approximations. By making use of the simplified analysis in the previous section, we will work out an approximate scheme that captures the essential details of the low-energy dynamics.

The nonperturbative arguments of Sec. III C may suggest that the transport due to the Fermi arcs is nondissipative. However, it is quite reasonable to suspect that the description of the Fermi arc states using the effective Hamiltonian (5) is inadequate. The point is that the corresponding approach completely ignores the possibility of the surface states scattering into the bulk. From a physics viewpoint, however, such scattering is unavoidable at least in certain regions of the phase space. In particular, this is the case for the surface states near the ends of the Fermi arcs, where they smoothly transform into the bulk states. As we argue below, the resulting non-decoupling of the surface and bulk sectors in the full theory is critical. It is responsible for dissipative transport properties.

The general definition of the conductivity in terms of the current-current correlation function (12) remains valid also in the full model (1). However, one has to modify the definition of the currents to account for the correct matrix structure of the vertices, i.e.,

$$j_x = -ev_F\psi^\dagger\sigma_x\psi, \quad (44)$$

$$j_z = -2e\gamma k_z\psi^\dagger\sigma_z\psi. \quad (45)$$

By taking into account the matrix structure of the vertices in these currents and the matrix structure of the surface state propagator (32), it is straightforward to show that two out of three possible components of the conductivity tensor are vanishing, i.e.,  $\sigma_{xz} = \sigma_{zz} = 0$ . The remaining nontrivial component of the DC conductivity tensor reads

$$\sigma_{xx}(\mathbf{r}) = -\lim_{\Omega \rightarrow 0} \frac{i}{\Omega} \Pi_{xx}(\mathbf{r}), \quad (46)$$

Note that the result may depend on the position vector  $\mathbf{r}$  (e.g., see Ref. [51]). In the coordinate space, the corresponding correlator is given by

$$\Pi_{xx}(\mathbf{r}) \simeq e^2 v_F^2 \Omega \int \frac{d\omega}{2\pi} \frac{\partial f(\omega)}{\partial \omega} \int d^3\mathbf{r}' \text{tr} [\langle \sigma_x(-i)G_s^A(\omega; \mathbf{r}, \mathbf{r}')\sigma_x(-i)G_s^R(\omega; \mathbf{r}', \mathbf{r}) \rangle_{\text{dis}}], \quad (47)$$

where we kept only the linear term in  $\Omega$ , which is relevant for the DC conductivity. In the last expression,  $f(\omega)$  is the Fermi-Dirac quasiparticle distribution function. In the limit of zero temperature, in particular, it is given by  $f_0(\omega) = \theta(\mu - \omega)$ .

It is understood that the full (advanced and retarded) propagators  $G_s^{A/R}(\omega; \mathbf{r}, \mathbf{r}')$  are calculated in the presence of disorder. The corresponding expressions could be formally obtained in the form of infinite series of diagrams with different number of insertions, representing scatterings on impurities, i.e.,

$$G \equiv \begin{array}{c} \times \\ | \\ \longrightarrow + \longrightarrow \bullet \longrightarrow + \longrightarrow \bullet \bullet \longrightarrow + \longrightarrow \bullet \bullet \bullet \longrightarrow + \dots \end{array} \quad (48)$$

After substituting the propagators into the expression for the correlation function (47) and averaging over the disorder, we obtain [47]

$$\Pi_{xx}(\mathbf{r}) = \begin{array}{c} \text{Diagram 1} + \text{Diagram 2} + \text{Diagram 3} \\ + \text{Diagram 4} + \text{Diagram 5} + \text{Diagram 6} + \dots \end{array} \quad (49)$$

where the dashed line represents the impurity correlation function (11) and the double solid line represents the disorder-averaged quasiparticle propagators  $\langle G \rangle_{\text{dis}}$ . In the rainbow approximation, the latter is given by

$$\langle G \rangle_{\text{dis}} \equiv \begin{array}{c} \text{Diagram 1} \\ = \text{Diagram 2} + \text{Diagram 3} \end{array} \quad (50)$$

It should be noted that, in the last equation, we ignored a correction to the self-energy linear in the impurity potential. As we will show in Sec. V A, it has the form  $\Sigma^{(1)} = n_{\text{imp}}u_0$ . The effect of such a term is to shift the value of the chemical potential,  $\mu^* = \mu - n_{\text{imp}}u_0$ . Clearly, such a redefinition has no qualitative importance and, thus, will be ignored.

In three-dimensional systems, the contributions of the diagrams with crossing impurity lines, e.g., see the second row of diagrams in Eq. (49), are usually suppressed compared to the diagrams without crossing lines [47]. Since in the present model there are no strict one-dimensional chiral fermions that are fully decoupled from the bulk states, its dynamics should be close to a three dimensional one. Therefore one could expect that omitting the impurity-crossing diagrams should provide at least a reasonable approximation in this case.

Then, the current-current correlation function takes the following diagrammatic form:

$$\Pi_{xx} = \text{Diagram} = -e^2 v_F^2 \Omega \int \frac{d\omega}{2\pi} \frac{\partial f(\omega)}{\partial \omega} \int d^3 \mathbf{r}' d^3 \mathbf{r}_1 d^3 \mathbf{r}_2 \text{tr} [\sigma_x \langle G_s^A(\omega; \mathbf{r}, \mathbf{r}_1) \rangle_{\text{dis}} \Lambda_x(\omega; \mathbf{r}_1, \mathbf{r}', \mathbf{r}_2) \langle G_s^R(\omega; \mathbf{r}_2, \mathbf{r}) \rangle_{\text{dis}}], \quad (51)$$

where we introduced the vertex function in the ladder approximation:

$$\Lambda_x(\omega; \mathbf{r}_1, \mathbf{r}', \mathbf{r}_2) \equiv \text{Diagram} = \text{Diagram} + \text{Diagram} \quad (52)$$

The corresponding explicit expression reads

$$\Lambda_x(\omega; \mathbf{r}_1, \mathbf{r}', \mathbf{r}_2) = \sigma_x \delta(\mathbf{r}_1 - \mathbf{r}') \delta(\mathbf{r}' - \mathbf{r}_2) + D(\mathbf{r}_1, \mathbf{r}_2) \int d^3 \mathbf{r}'_1 d^3 \mathbf{r}'_2 (-i) \langle G_s^A(\omega; \mathbf{r}_1, \mathbf{r}'_1) \rangle_{\text{dis}} \Lambda_x(\omega; \mathbf{r}'_1, \mathbf{r}', \mathbf{r}'_2) (-i) \langle G_s^R(\omega; \mathbf{r}'_2, \mathbf{r}_2) \rangle_{\text{dis}}. \quad (53)$$

By switching to a mixed coordinate and momentum space representation, we rewrite the expression for the conductivity in the following form:

$$\sigma(\mathbf{q}_{\parallel}, y) = - \lim_{\Omega \rightarrow 0} \frac{i}{\Omega} \Pi(\mathbf{q}_{\parallel}, y), \quad (54)$$

where the corresponding current-current correlator is given by

$$\begin{aligned} \Pi(\mathbf{q}_{\parallel}, y) &= -e^2 v_F^2 \Omega \int \frac{d\omega}{2\pi} \frac{\partial f(\omega)}{\partial \omega} \int \frac{d\mathbf{k}_{\parallel}}{(2\pi)^2} \int dy' dy_1 dy_2 \text{tr} [\sigma_x \langle G_s^A(\omega; \mathbf{k}_{\parallel}, y, y_1) \rangle_{\text{dis}} \\ &\times \Lambda_x(\omega; \mathbf{k}_{\parallel}, \mathbf{k}_{\parallel} - \mathbf{q}_{\parallel}, y_1, y', y_2) \langle G_s^R(\omega; \mathbf{k}_{\parallel} - \mathbf{q}_{\parallel}, y_2, y) \rangle_{\text{dis}}]. \end{aligned} \quad (55)$$

In this study we are interested in the DC electrical conductivity. By taking into account that the corresponding transport coefficient describes the linear response of the system to a spatially homogeneous electric field, we set  $\mathbf{q}_{\parallel} = 0$ . Then, the vertex function satisfies the following equation:

$$\begin{aligned} \Lambda_x(\omega; \mathbf{k}_{\parallel}, \mathbf{k}_{\parallel}, y_1, y', y_2) &= \sigma_x \delta(y_1 - y') \delta(y' - y_2) + \int \frac{d\mathbf{l}_{\parallel}}{(2\pi)^2} \int dy'_1 dy'_2 D(\mathbf{k}_{\parallel} - \mathbf{l}_{\parallel}, y_1, y_2) \\ &\times (-i) \langle G_s^A(\mathbf{l}_{\parallel}, \omega; y_1, y'_1) \rangle_{\text{dis}} \Lambda_x(\omega; \mathbf{l}_{\parallel}, \mathbf{l}_{\parallel}, y'_1, y', y'_2) (-i) \langle G_s^R(\omega; \mathbf{l}_{\parallel}, y'_2, y_2) \rangle_{\text{dis}}. \end{aligned} \quad (56)$$

In order to calculate the conductivity in this approximation, therefore, we would first need to calculate the full quasiparticle propagator averaged over the disorder and then solve Eq. (56) for the full vertex function. Finally, the knowledge of the propagator and vertex will allow us to derive the expression for the correlator (55) and, therefore, the conductivity (54). Thus, in the next two subsections, we calculate both of them using standard methods.

### A. Self-energy and full quasiparticle propagator

In this subsection we calculate the self-energy and determine the width of the Fermi arc states in the full model (1). To start with, let us remind that the surface and bulk Green's functions in the absence of disorder are given by Eqs. (32) and (33), respectively.

Here we will determine the full Green's function for the surface states by calculating their self-energy to the quadratic order in the disorder strength  $u_0$ . Formally, the definition for the self-energy is the same as in Eq. (24). However, one has to keep in mind that the internal quasiparticle propagator in the corresponding diagram could be either the surface or bulk one. Therefore, there are different types of contributions to the final result coming from the diagrams with the bulk or surface internal lines.

By expanding the full Green's function to the second order in powers of the disorder strength  $u_0$ , see Eqs. (48) and (50), we derive the following result:

$$(-i)G(\omega, \mathbf{k}_{\parallel}, \mathbf{k}'_{\parallel}; y, y') = S^{(0)}(\omega, \mathbf{k}_{\parallel}, \mathbf{k}'_{\parallel}; y, y') + S^{(1)}(\omega, \mathbf{k}_{\parallel}, \mathbf{k}'_{\parallel}; y, y') + S^{(2)}(\omega, \mathbf{k}_{\parallel}, \mathbf{k}'_{\parallel}; y, y'), \quad (57)$$

where

$$S^{(0)}(\omega, \mathbf{k}_{\parallel}, \mathbf{k}'_{\parallel}; y, y') = (2\pi)^2 \delta(\mathbf{k}_{\parallel} - \mathbf{k}'_{\parallel}) (-i) S_s(\omega, \mathbf{k}_{\parallel}; y, y'), \quad (58)$$

and  $S_s(\omega, \mathbf{k}_{\parallel}; y, y')$  is the surface Green's function given by (32). The first order correction is given by

$$\begin{aligned} S^{(1)}(\omega, \mathbf{k}_{\parallel}, \mathbf{k}'_{\parallel}; y, y') &= \sum_j \int dy'' (-i) S_s(\omega, \mathbf{k}_{\parallel}; y, y'') u_0 \delta(y'' - y_j) e^{-ir_j(\mathbf{k}_{\parallel} - \mathbf{k}'_{\parallel})} (-i) S_s(\omega, \mathbf{k}'_{\parallel}; y'', y') \\ &= \sum_j \int dy'' \frac{p(k_z)(1 + \sigma_x) e^{-(y+y'')p(k_z)}}{\omega + i0 + \mu - v_F k_x} u_0 \delta(y'' - y_j) e^{-ir_j(\mathbf{k}_{\parallel} - \mathbf{k}'_{\parallel})} \frac{p(k'_z)(1 + \sigma_x) e^{-(y''+y')p(k'_z)}}{\omega + i0 + \mu - v_F k'_x}. \end{aligned} \quad (59)$$

By averaging over the impurities using the prescription in Eq. (10) and integrating over  $y''$ , we obtain

$$\begin{aligned} \langle S^{(1)}(\omega, \mathbf{k}_{\parallel}, \mathbf{k}'_{\parallel}; y, y') \rangle_{\text{dis}} &= \sum_j \frac{1}{V} u_0 (2\pi)^2 \delta(\mathbf{k}_{\parallel} - \mathbf{k}'_{\parallel}) \frac{p(k_z)}{2} \frac{(1 + \sigma_x)^2}{(\omega + i0 + \mu - v_F k_x)^2} e^{-(y+y')p(k_z)} \\ &= n_{\text{imp}} u_0 \frac{e^{(y+y')p(k_z)}}{2p(k_z)} (2\pi)^2 \delta(\mathbf{k}_{\parallel} - \mathbf{k}'_{\parallel}) (-i) S_s(\omega, \mathbf{k}_{\parallel}; y, y') (-i) S_s(\omega, \mathbf{k}_{\parallel}; y', y). \end{aligned} \quad (60)$$

Let us note that, in order to extract the correct definition of the self-energy from this result, it is instructive to compare the above expression with the formal expansion of the surface Green's function to linear order in  $\Sigma(k_z)$ ,

$$\begin{aligned} \frac{p(k_z)(1 + \sigma_x) e^{-(y+y')p(k_z)}}{\omega + \mu - v_F k_x - \Sigma(k_z)} &= \frac{p(k_z)(1 + \sigma_x) e^{-(y+y')p(k_z)}}{\omega + \mu - v_F k_x} + \frac{p(k_z)(1 + \sigma_x) e^{-(y+y')p(k_z)}}{(\omega + \mu - v_F k_x)^2} \Sigma(k_z) \\ &= (-i) S_s(\omega, \mathbf{k}_{\parallel}; y', y) + \frac{e^{(y+y')p(k_z)}}{2p(k_z)} (-i) S_s(\omega, \mathbf{k}_{\parallel}; y', y) \Sigma(k_z) (-i) S_s(\omega, \mathbf{k}_{\parallel}; y', y). \end{aligned} \quad (61)$$

Here we took into account that  $(1 + \sigma_x)^2 = 2(1 + \sigma_x)$ . By comparing this expansion with the result in Eq. (60), we extract the following first order correction to the real part of self energy:

$$\Sigma^{(1)}(\mathbf{k}_{\parallel}) = n_{\text{imp}} u_0. \quad (62)$$

This result is qualitatively the same as the leading order correction to the self-energy in three dimensional theories [47]. Its effect is to shift the chemical potential from  $\mu$  to  $\mu^*$ , where

$$\mu^* \equiv \mu - \Sigma^{(1)}(\mathbf{k}_{\parallel}) = \mu - n_{\text{imp}} u_0. \quad (63)$$

In the remainder of this paper, we will ignore this correction to the chemical potential (or the difference between  $\mu$  and  $\mu^*$ ) due to its qualitative unimportance.

Next, we calculate the second order correction  $S^{(2)}(\omega, \mathbf{k}_{\parallel}, \mathbf{k}'_{\parallel}; y, y')$  using the *surface* Green's function as an intermediate line in the second-order diagram in Eq. (50), i.e.,

$$\begin{aligned} S_s^{(2)}(\omega, \mathbf{k}_{\parallel}, \mathbf{k}'_{\parallel}; y, y') &= \sum_j \int dy_1 dy_2 \int \frac{d\mathbf{q}_{\parallel}}{(2\pi)^2} (-i) S(\omega, \mathbf{k}_{\parallel}; y, y_1) u_0 \delta(y_1 - y_j) e^{-ir_j(\mathbf{k}_{\parallel} - \mathbf{q}_{\parallel})} (-i) S(\omega, \mathbf{q}_{\parallel}; y_1, y_2) \\ &\times u_0 \delta(y_2 - y_j) e^{-ir_j(\mathbf{q}_{\parallel} - \mathbf{k}'_{\parallel})} (-i) S(\omega, \mathbf{k}'_{\parallel}; y_2, y') = \sum_j u_0^2 e^{-ir_j(\mathbf{k}_{\parallel} - \mathbf{k}'_{\parallel})} e^{-p(k_z)(y+y')} \\ &\times \int \frac{d\mathbf{q}_{\parallel}}{(2\pi)^2} e^{-2p(k_z)y_j - 2p(q_z)y_j} \frac{(1 + \sigma_x)^3 [p(k_z)]^2 p(q_z)}{(\omega + i0 + \mu - v_F k_x)^2 (\omega + i0 + \mu - v_F q_x)}. \end{aligned} \quad (64)$$

After the averaging over impurities, we then obtain

$$\begin{aligned} \langle S_s^{(2)}(\omega, \mathbf{k}_{\parallel}, \mathbf{k}'_{\parallel}; y, y') \rangle_{\text{dis}} &= \frac{N_{\text{imp}}}{V} u_0^2 \delta(\mathbf{k}_{\parallel} - \mathbf{k}'_{\parallel}) \int d\mathbf{q}_{\parallel} \frac{(1 + \sigma_x)^3 e^{-p(k_z)(y+y')}}{(\omega + i0 + \mu - v_F k_x)^2 (\omega + i0 + \mu - v_F q_x)} \frac{[p(k_z)]^2 p(q_z)}{2p(k_z) + 2p(q_z)} \\ &= \frac{-i\pi}{v_F} n_{\text{imp}} u_0^2 \delta(\mathbf{k}_{\parallel} - \mathbf{k}'_{\parallel}) \frac{(1 + \sigma_x)^3 e^{-p(k_z)(y+y')}}{(\omega + i0 + \mu - v_F k_x)^2} \frac{[p(k_z)]^2}{2} \int_{-\sqrt{m}}^{\sqrt{m}} dq_z \left[ 1 - \frac{p(k_z)}{p(k_z) + p(q_z)} \right]. \end{aligned} \quad (65)$$

Here we took into account the retarded nature of the Green's functions and used the finiteness of the  $z$ -component of momentum. The latter condition stems from the normalizability of the wave function. Furthermore, the result in Eq. (65) can be rewritten as follows:

$$\begin{aligned} \langle S_s^{(2)}(\omega, \mathbf{k}_{\parallel}, \mathbf{k}'_{\parallel}; y, y') \rangle_{\text{dis}} &= \frac{-i}{4\pi v_F} n_{\text{imp}} u_0^2 (2\pi)^2 \delta(\mathbf{k}_{\parallel} - \mathbf{k}'_{\parallel}) e^{p(k_z)(y+y')} (-i) S(\omega, \mathbf{k}_{\parallel}; y, y') (-i) S(\omega, \mathbf{k}_{\parallel}; y', y) \\ &\times \left[ 2\sqrt{m} + \frac{2v_F p(k_z)}{\sqrt{-\gamma v_F p(k_z) - m\gamma^2}} \arctan \left( \frac{\sqrt{\gamma m}}{\sqrt{-v_F p(k_z) - \gamma m}} \right) \right]. \end{aligned} \quad (66)$$

Thus, we finally extract the second order correction to the self-energy

$$\Sigma_s^{(2)}(\mathbf{k}_{\parallel}) = -i \frac{\gamma(m - k_z^2)}{\pi v_F^2} n_{\text{imp}} u_0^2 \left[ \sqrt{m} - \frac{(k_z^2 - m)}{\sqrt{k_z^2 - 2m}} \arctan \left( \frac{\sqrt{m}}{\sqrt{k_z^2 - 2m}} \right) \right]. \quad (67)$$

As we see, this correction is imaginary and has a nontrivial dependence on the wave vector  $k_z$ . This means that the surface quasiparticles receive a nonzero width contribution, given by

$$\Gamma_s(k_z) = \frac{\gamma(m - k_z^2)}{\pi v_F^2} n_{\text{imp}} u_0^2 \left[ \sqrt{m} - \frac{(k_z^2 - m)}{\sqrt{k_z^2 - 2m}} \arctan \left( \frac{\sqrt{m}}{\sqrt{k_z^2 - 2m}} \right) \right]. \quad (68)$$

We note, however, that the above result is not complete yet. To the same second order in the disorder strength, there is also another contribution, in which the intermediate line in the second-order diagram in Eq. (50) is given by the *bulk* Green's function (33), i.e.,

$$\begin{aligned} \langle S_b^{(2)}(\omega, \mathbf{k}_{\parallel}, \mathbf{k}'_{\parallel}; y, y') \rangle_{\text{dis}} &= \left\langle \sum_j \int dy_1 dy_2 \int \frac{d\mathbf{q}_{\parallel}}{(2\pi)^2} (-i) S(\omega, \mathbf{k}_{\parallel}; y, y_1) u_0 \delta(y_1 - y_j) e^{-i\mathbf{r}_j(\mathbf{k}_{\parallel} - \mathbf{q}_{\parallel})} \right. \\ &\times \left. (-i) S_b(\omega, \mathbf{q}_{\parallel}; y_1 - y_2) u_0 \delta(y_2 - y_j) e^{-i\mathbf{r}_j(\mathbf{q}_{\parallel} - \mathbf{k}'_{\parallel})} (-i) S(\omega, \mathbf{k}'_{\parallel}; y_2, y') \right\rangle_{\text{dis}}. \end{aligned} \quad (69)$$

After simplification, this result can be rewritten equivalently as follows:

$$\begin{aligned} \langle S_b^{(2)}(\omega, \mathbf{k}_{\parallel}, \mathbf{k}'_{\parallel}; y, y') \rangle_{\text{dis}} &= n_{\text{imp}} u_0^2 (2\pi)^2 \delta(\mathbf{k}_{\parallel} - \mathbf{k}'_{\parallel}) e^{p(k_z)(y+y')} (-i) S(\omega, \mathbf{k}_{\parallel}; y, y') (-i) S(\omega, \mathbf{k}_{\parallel}; y', y) \frac{e^{(y+y')p(k_z)}}{2p(k_z)} \\ &\times \int \frac{d\mathbf{q}}{(2\pi)^3} \frac{[\omega + \mu + v_F q_x \sigma_x]}{(\omega + \mu)^2 - \gamma^2 (q_z^2 - m)^2 - v_F^2 q_{\parallel}^2 + i0 \text{sign}(\omega + \mu)}. \end{aligned} \quad (70)$$

While the general result is rather complicated, we can extract its imaginary part analytically by using the Sokhotsky's formula. After integrating over  $\mathbf{q}$ , we derive the following result:

$$\text{Im} \left[ \Sigma_b^{(2)}(\omega) \right] = -n_{\text{imp}} u_0^2 \frac{|\omega + \mu|}{4v_F^2 \pi} \left[ \sqrt{m + \frac{|\omega + \mu|}{\gamma}} - \theta \left( m - \frac{|\omega + \mu|}{\gamma} \right) \sqrt{m - \frac{|\omega + \mu|}{\gamma}} \right], \quad (71)$$

which has a nontrivial dependence on the energy  $\omega$ . The corresponding contribution to the quasiparticle width is given by

$$\Gamma_b(\omega) \equiv n_{\text{imp}} u_0^2 \frac{|\omega + \mu|}{4v_F^2 \pi} \left[ \sqrt{m + \frac{|\omega + \mu|}{\gamma}} - \theta \left( m - \frac{|\omega + \mu|}{\gamma} \right) \sqrt{m - \frac{|\omega + \mu|}{\gamma}} \right]. \quad (72)$$

Finally, by combining the results in Eqs. (68) and (72), we derive the total quasiparticle width of surface quasiparticles, i.e.,

$$\Gamma(\omega; k_z) = \Gamma_s(k_z) + \Gamma_b(\omega). \quad (73)$$

The corresponding full surface Green's function, averaged over disorder, is given by

$$\langle G(\omega, \mathbf{k}_{\parallel}; y, y') \rangle_{\text{dis}} \simeq \frac{2ip(k_z)e^{-(y+y')p(k_z)}}{\omega + \mu - v_F k_x + i\Gamma(\omega, k_z)} \frac{1 + \sigma_x}{2}. \quad (74)$$

### B. Vertex correction

In this subsection we calculate the full vertex function in the ladder approximation. The explicit form of the equation for the vertex (56) reads

$$\begin{aligned} \Lambda_x(\omega; \mathbf{k}_{\parallel}, \mathbf{k}_{\parallel}, y_1, y', y_2) &= \sigma_x \delta(y_1 - y_2) \delta(y' - y_1) + n_{\text{imp}} u_0^2 \delta(y_1 - y_2) \int \frac{dl_{\parallel}}{(2\pi)^2} \int dy'_1 dy'_2 \frac{(1 + \sigma_x) p(l_z) e^{-(y_1+y'_1)p(l_z)}}{[\omega - v_F l_x - i\Gamma(\omega, l_z)]} \\ &\times \Lambda_x(\omega, \mathbf{l}_{\parallel}, \mathbf{l}_{\parallel}; y'_1, y', y'_2) \frac{(1 + \sigma_x) p(l_z) e^{-(y_2+y'_2)p(l_z)}}{[\omega - v_F l_x + i\Gamma(\omega, l_z)]}. \end{aligned} \quad (75)$$

The matrix structure on the right hand side of the above equation suggests that the solution for the vertex function should take the following form:

$$\Lambda_x(\omega, \mathbf{k}_{\parallel}, \mathbf{k}_{\parallel}; y_1, y', y_2) = \sigma_x \delta(y_1 - y_2) \delta(y' - y_1) + \delta(y_1 - y_2) \frac{1 + \sigma_x}{2} f(\omega, y_1, y'). \quad (76)$$

By substituting such an ansatz into Eq. (75), we find that the unknown function  $f(\omega, y_1, y')$  should satisfy the following equation:

$$f(\omega, y_1, y') = F(\omega, y_1, y') + \int dy'_1 F(\omega, y_1, y'_1) f(\omega, y'_1, y'), \quad (77)$$

where

$$F(\omega, y_1, y') \equiv \frac{2n_{\text{imp}} u_0^2}{v_F} \int_{-\sqrt{m}}^{\sqrt{m}} \frac{dl_z}{2\pi} \frac{p^2(l_z) e^{-2(y_1+y')p(l_z)}}{\Gamma(\omega, l_z)}. \quad (78)$$

By compiling this function numerically, we found that it can be approximated quite well by the following fit:

$$F(\omega, y_1, y') \approx \frac{a(\omega)}{1 + d(\omega)(y_1 + y') + b(\omega)(y_1 + y')^2}, \quad (79)$$

where the three fitting parameters are functions of  $\omega$ . At  $\omega = 0$ , for example, their numerical values are  $a(0) = 0.106 \text{ \AA}^{-1}$  and  $b(0) = 0.004 \text{ \AA}^{-2}$ , and  $d(0) = 0.032 \text{ \AA}^{-1}$ .

Eq. (77) is a Fredholm integral equation of the second kind. When the norm of the kernel is sufficiently small, i.e.,

$$N_F(\omega) \equiv \left( \int_0^{\infty} dy \int_0^{\infty} dy' F^2(\omega, y, y') \right)^{1/2} < 1, \quad (80)$$

its solution can be obtained by iterations. The formal result in this case reads

$$f(\omega, y, y') = F(\omega, y, y') + \sum_{n=1}^{\infty} \int_0^{\infty} dy'' K_n(\omega, y, y'') F(\omega, y'', y'), \quad (81)$$

where, by definition,  $K_1(\omega, y, y') \equiv F(\omega, y, y')$  and

$$K_n(\omega, y, y') = \int_0^{\infty} dy'' F(\omega, y, y'') K_{n-1}(\omega, y'', y'). \quad (82)$$

This solution defines a convergent series at sufficiently large values of  $\omega$  [e.g., for  $\omega \approx \gamma m/2$ ,  $N_F(\omega) \approx 0.8$ ]. For small  $\omega$  (i.e.,  $\omega \lesssim 0.04\gamma m$ ), an alternative algorithm for solving the corresponding Fredholm equation should be utilized.

### C. Fermi arc conductivity

By combining the results of the previous two subsections, in this subsection we calculate the conductivity of the Fermi arc states.

We start by presenting the mixed coordinate-momentum space representation of the spectral function for the surface Fermi arc states,

$$\begin{aligned} A(\omega, \mathbf{k}_{\parallel}; y, y') &= \frac{i}{2\pi} [\langle G^R(\omega, \mathbf{k}_{\parallel}; y, y') \rangle_{\text{dis}} - \langle G^A(\omega, \mathbf{k}_{\parallel}; y, y') \rangle_{\text{dis}}]_{\mu=0} \\ &= \frac{i}{\pi} (1 + \sigma_x) p(k_z) e^{-(y+y')p(k_z)} \frac{\Gamma(\omega, k_z)}{(\omega - v_F k_x)^2 + \Gamma^2(\omega, k_z)} \theta(m - k_z^2), \end{aligned} \quad (83)$$

where  $\Gamma(\omega, k_z)$  is given by Eq. (73). The corresponding Green's function can be restored from this spectral function by using the relation in Eq. (16).

The  $xx$ -component of the DC conductivity tensor is defined by Eq. (54) evaluated at  $\mathbf{q}_{\parallel} = 0$ . By making use of the Green's function representation in terms of the spectral function (83), we rewrite the expression for the conductivity as follows:

$$\begin{aligned} \sigma_{xx}^{\text{tot}}(y) &= - \lim_{\Omega \rightarrow 0} \frac{i}{\Omega} e^2 v_F^2 T \sum_{l=-\infty}^{\infty} \int \frac{d\mathbf{k}_{\parallel}}{(2\pi)^2} \int \int \int dy' dy_1 dy_2 \int \int d\omega d\omega' \\ &\times \frac{\text{tr} [\sigma_x A(\omega, \mathbf{k}_{\parallel}; y, y_1) \Lambda_x(\omega, \omega'; \mathbf{k}_{\parallel}, \mathbf{k}_{\parallel}, y_1, y', y_2) A(\omega', \mathbf{k}_{\parallel}; y_2, y)]}{(i\omega_l + \mu - \omega)(i\omega_l - \Omega - i0 + \mu - \omega')}, \end{aligned} \quad (84)$$

where the vertex for  $\omega = \omega'$  is given by Eq. (56). We emphasize that the knowledge of the vertex correction at  $\omega = \omega'$  is sufficient for calculating the real part of the DC conductivity.

To start with, let us first calculate the real part of the  $xx$ -component of the conductivity tensor (84) without the vertex correction. In other words, we use the bare vertex,  $\Lambda_x^{(0)}(\omega; \mathbf{k}_{\parallel}, \mathbf{k}_{\parallel}, y_1, y', y_2) = \sigma_x \delta(y' - y_1) \delta(y' - y_2)$ . The corresponding result reads

$$\begin{aligned} \Re \sigma_{xx}^{(0)}(y) &= e^2 v_F^2 \int_0^{\infty} dy' \int_{-\sqrt{m}}^{\sqrt{m}} \frac{dk_z}{2\pi} \int \frac{dk_x d\omega}{(2\pi)^2} \frac{4p^2(k_z)}{4T \cosh^2\left(\frac{\omega - \mu}{2T}\right)} \frac{e^{-2(y+y')p(k_z)}}{(\omega - v_F k_x)^2 + \Gamma^2(\omega, k_z)} \\ &= \frac{e^2 v_F}{4\pi^2} \int_{-\sqrt{m}}^{\sqrt{m}} dk_z \int d\omega \frac{p(k_z)}{4T \cosh^2\left(\frac{\omega - \mu}{2T}\right)} \frac{e^{-2(y+y')p(k_z)}}{\Gamma(\omega, k_z)}. \end{aligned} \quad (85)$$

The first-order correction to this result is given by

$$\begin{aligned} \Re \sigma_{xx}^{(1)}(y) &= e^2 v_F^2 \int \frac{d\omega}{2\pi} \frac{1}{4T \cosh^2\left(\frac{\omega - \mu}{2T}\right)} \int dy' dy_1 dy_2 \int \frac{d\mathbf{k}_{\parallel}}{(2\pi)^2} \text{tr} \left[ \sigma_x \frac{p(k_z)(1 + \sigma_x) e^{-(y+y_1)p(k_z)} \Gamma(\omega, k_z)}{(\omega - v_F k_x)^2 + \Gamma^2(\omega, k_z)} \right. \\ &\times \left. \delta(y_1 - y_2) n_{\text{imp}} u_0^2 \int \frac{dl_{\parallel}}{(2\pi)^2} \frac{(1 + \sigma_x)^2 \sigma_x p^2(l_z) e^{-2(y'+y_1)p(l_z)}}{(\omega - v_F l_x)^2 + \Gamma^2(\omega, l_z)} \frac{p(k_z)(1 + \sigma_x) e^{-(y_2+y)p(k_z)} \Gamma(\omega, k_z)}{(\omega - v_F k_x)^2 + \Gamma^2(\omega, k_z)} \right] \\ &= \frac{e^2}{16\pi^3} n_{\text{imp}} u_0^2 \int d\omega \frac{1}{4T \cosh^2\left(\frac{\omega - \mu}{2T}\right)} \int_{-\sqrt{m}}^{\sqrt{m}} \int_{-\sqrt{m}}^{\sqrt{m}} \frac{dk_z dl_z}{\Gamma(\omega, k_z) \Gamma(\omega, l_z)} \frac{e^{-2yp(k_z)} p(l_z) p^2(k_z)}{[p(k_z) + p(l_z)]}. \end{aligned} \quad (86)$$

Here we took into account the leading-order correction to the vertex with a single impurity correlator bridging the incoming fermion lines in the diagram.

Our numerical results for the zero temperature conductivity of the surface Fermi arc states are summarized in Fig. 6. In each panel, we show (i) the leading order result  $\Re \sigma_{xx}^{(0)}(y)$  without any vertex corrections (blue dashed lines), (ii) the first order correction  $\Re \sigma_{xx}^{(1)}(y)$  (red dotted lines), as well as (iii) the total conductivity  $\Re \sigma_{xx}^{\text{tot}}(y) \equiv \Re \sigma_{xx}^{(0)}(y) + \Re \sigma_{xx}^{(1)}(y)$  (black solid lines). For the strength of the disorder potential and the density of impurities, we used the values  $u_0 = 0.1 \text{ eV } \text{\AA}^3$  and  $n_{\text{imp}} = 10^{-3} \text{ \AA}^{-3}$ , respectively.

The left panel in Fig. 6 shows the real part of the conductivity as a function of the (dimensional) distance  $y$ , measured from the surface into the bulk. The result is shown for a fixed value of the chemical potential,  $\mu = 0.05 \text{ eV}$ . This choice of  $\mu$  is sufficiently large to be still marginally in the regime of reliable perturbative calculations, where the vertex correction is not too large. This is also confirmed by the fact that the leading order result dominates the

total conductivity. From the functional dependence we see that, as expected, the Fermi arc conductivity takes the highest value on the surface ( $y = 0$ ) and rapidly decreases as the function of  $y$ .

The dependence of the conductivity on the dimensionless chiral shift parameter (or the arcs length)  $\gamma m/\mu$  is shown in the middle panel of Fig. 6. The results are plotted for  $y = 0$  and the same fixed value of the chemical potential,  $\mu = 0.05$  eV. Despite the fact that the quasiparticle width (68) has a very nontrivially dependence on the chiral shift parameter  $m$ , the conductivity appears to always grow with  $m$ . It is also interesting to note that the slopes of the functional dependence are different at small and large values of  $\gamma m/\mu$ , showing a characteristic (van Hove) kink at  $m = \mu/\gamma$ . The existence of such a kink can be explained by the Lifshitz transition [48]. Indeed, as one can see from the left panel of Fig. 1, two disjoint sheets of the Fermi surface merge into a single one at  $m = \mu/\gamma$  resulting in the van Hove kink. Note that the corresponding phenomenon was observed in three-dimensional Dirac semimetal Na<sub>3</sub>Bi [49].

The right panel in Fig. 6 shows the conductivity as a function of the (dimensional) chemical potential  $\mu$  at fixed position  $y = 0$  (on the surface). One of the main features of the corresponding result is that the total surface conductivity decreases with  $\mu$ . At first sight, this may appear counterintuitive. However, this is indeed the case and the explanation is quite simple. Because of the specific mechanism of dissipation, i.e., scattering of the surface Fermi arc states into the bulk, the width of surface quasiparticles grows when the density of bulk states increases. Indeed, such an increase expands the available phase space for scattered states into the bulk and, thus, damps the surface conductivity.

From the functional dependence of the conductivity on the chemical potential shown in the right panel of Fig. 6, we observe another interesting detail. In agreement with our analytical estimates in Sec. VB, the validity of the perturbative regime is limited only to the case of sufficiently large energies, or chemical potentials,  $\mu\gamma/v_F^2 \gtrsim 0.05$ , where the vertex corrections are under control. For smaller values of  $\mu$ , a nonperturbative solution of the integral equation for the vertex function (77) is needed. This is also supported by the calculated dependence of the surface conductivity on  $\mu$ , which reveals that the leading order conductivity and the first correction become comparable at  $\mu\gamma/v_F^2 \ll 0.05$ .

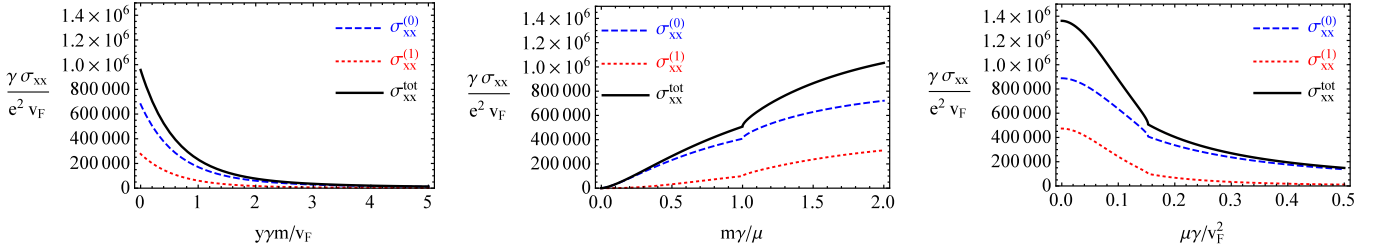


FIG. 6: (Color online) The real part of the surface conductivity at  $T = 0$  as a function of distance from the surface  $y$  (left panel), the dimensionless chiral shift parameter  $m$  (middle panel), and the chemical potential  $\mu$  (right panel). In the left and middle panels  $\mu = 0.05$  eV, in the middle and right panels  $y = 0$ . The other model parameters are  $u_0 = 0.1$  eV  $\text{\AA}^3$  and  $n_{\text{imp}} = 10^{-3}$   $\text{\AA}^{-3}$ .

The finite temperature results for the conductivity due to surface Fermi arc states are shown in Fig. 7 for  $y = 0$  and several representative values of parameters. By comparing the temperature dependence of the conductivity at different values of the chemical potentials, we find that there are two qualitatively different dynamical regimes. At sufficiently small values of  $\mu$  (i.e.,  $\mu\gamma/v_F^2 \lesssim 0.06$ ), the conductivity monotonically decreases with temperature. At larger values, there is a nonmonotonic dependence with a local maximum at a temperature that scales approximately as the chemical potential,

$$\frac{T_{\text{peak}}}{\gamma m} \approx \left( -0.2 + 4.1 \frac{\mu\gamma}{v_F^2} \right) \theta \left( \frac{\mu\gamma}{v_F^2} - 0.06 \right). \quad (87)$$

The underlying reason for the nonmonotonic behavior of the conductivity and the location of the maximum around  $T_{\text{peak}}$  are not completely transparent from the details of our analysis. It is natural to expect, however, that the roots of this dependence lie in the underlying mechanism of the dissipation of the surface states.

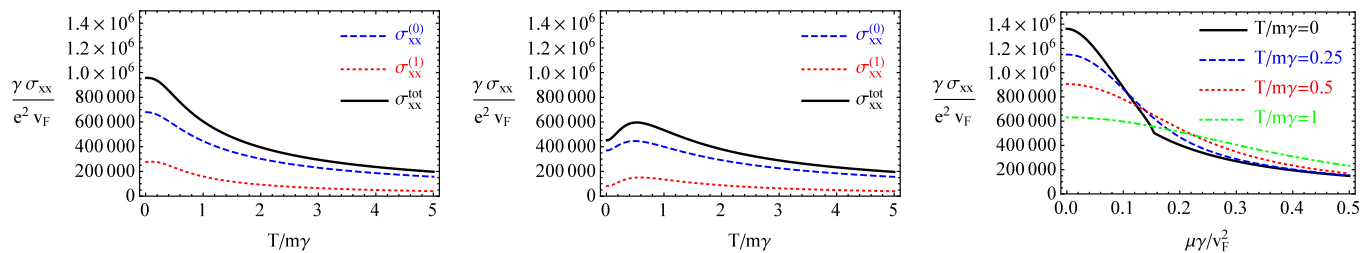


FIG. 7: (Color online) The real part of the surface conductivity as a function of temperature  $T$  at  $\mu = 0.05$  eV (left panel),  $\mu = 0.1$  eV (middle panel), as well as as a function of the chemical potential  $\mu$  at several different temperatures (right panel). The other model parameters are  $u_0 = 0.1$  eV  $\text{\AA}^3$  and  $n_{\text{imp}} = 10^{-3}$   $\text{\AA}^{-3}$ .

## VI. SUMMARY AND DISCUSSIONS

In this paper, we addressed the question whether the charge transport of the Fermi arcs in Weyl semimetals is dissipative or non-dissipative. Because of the topologically protected nature of the surface Fermi arc states, one would naively expect that the Fermi arc transport should be non-dissipative. We found, however, that the transport is, in fact, dissipative. The fundamental physical reason for the dissipation is the presence of gapless bulk states in Weyl semimetals, whose low-energy dynamics is not fully decoupled from the surface Fermi arc states. Indeed, by making use of the simplest model of a short-ranged quenched disorder, we showed that the Fermi arc quasiparticles can scatter into the bulk states in addition to scattering into other surface Fermi arc states. This nondecoupling implies that there is no well-defined effective theory of Fermi arcs in Weyl semimetals in the presence of quenched disorder. The electronic scattering from the surface into the bulk and vice versa leads to the dephasing of the Fermi arc quasiparticles and dissipation. This is in contrast to the case of topological insulators, in which bulk states are gapped. It appears that our findings agree with the generic conclusions in Refs. [31, 42], claiming that an effective theory of surface states in gapless systems can not be formulated.

We calculated the Fermi arc conductivity of Weyl semimetals by making use of the Kubo linear-response theory and a simple continuum model of a semiinfinite Weyl semimetal with a pair of Weyl nodes. We calculated explicitly the Fermi arc quasiparticle width and found that there are contributions due to (i) the intra-arc scattering and (ii) the bulk dephasing of the Fermi arc states [see, Eqs. (68) and (72), respectively]. Furthermore, we calculated the Fermi arc conductivity explicitly and confirmed that the scattering of the Fermi arc quasiparticles into the bulk ones is indeed responsible for the *dissipative* transport. In the analysis, we used the current-current correlator with the vertex correction in the ladder approximation. We also showed that the corresponding correction may be important in certain regions of the parameter space.

Our results reveal that the Fermi arc conductivity at zero temperature decreases with the growth of chemical potential (see, the right panel of Fig. 6). This is explained by the associated increase of the Fermi arc quasiparticle width that grows with the density of states in the bulk. By noting that the ladder approximation for the vertex gradually deteriorates at small values of chemical potential  $\mu$ , our results for the conductivity are quantitatively reliable only at sufficiently large  $\mu$ . The results at small (vanishing) values of chemical potential  $\mu$  should, therefore, be treated as an extrapolation. We hope that it would be possible to address the corresponding regime in the future by using a non-perturbative resummation for the vertex function. In this paper, we also analyzed the temperature dependence of the Fermi arc conductivity, which appears to be a decreasing function of  $T$  when the chemical potential is sufficiently small (i.e.,  $\mu\gamma/v_F^2 \lesssim 0.06$ ). At larger value of  $\mu$ , the temperature dependence of the conductivity is nonmonotonic with a local maximum at a temperature that scales approximately as the chemical potential, see Fig. 7. This suggests a certain nontrivial competition between the phase space of the bulk states and the thermal effects. The precise nature of the corresponding mechanism, however, remains somewhat elusive. We hope to consider this issue in more detail somewhere else.

As we showed in our study, the region of small chemical potential  $\mu$  is peculiar. This is due to the fact that the vertex function becomes large in the region of small energies and the leading-order perturbative treatment is insufficient. In this case, a nonperturbative analysis of the integral equation for the vertex (75) is needed. Finally, there is an interesting question what happens in the case where the chemical potential is zero. Since the Fermi arc width decreases as chemical potential decrease, one would naively think that the Fermi arc conductivity blows up at  $\mu \rightarrow 0$ . However, according to the studies performed in Refs. [50] and [51], there is still a non-zero density of the bulk states in a disordered Weyl semimetal at zero chemical potential. In the case of charged impurities, the nonvanishing bulk density of states is realized due to the formation of electron/hole puddles [51]. The low energy behaviour of a

Weyl semimetal with local impurities is dominated by rare region effects, which are essentially nonperturbative [50]. Thus, the bulk states in disordered Weyl semimetals are present even at zero chemical potential. This suggests that the Fermi arc states always couple to the bulk ones, and the Fermi arc conductivity is always finite.

As is clear, the model used in this paper is quite simple and may not describe perfectly the transport of the Fermi arcs in real materials. In order to fully appreciate its strengths and limitations, therefore, it is pertinent to discuss the features of the model in more detail. For the sake of clarity, we studied a model with only one Fermi arc. In realistic Weyl semimetals (e.g., TaAs, TaP, NbAs, and NbP) there are usually more Fermi arcs, sometimes up to 12 [8, 9]. For the dissipation mechanism that we discussed, this is not very important, of course. However, the existence of numerous arcs opens the possibility for scattering processes between different Fermi arcs. Qualitatively, such additional processes can only increase surface quasiparticle width and, therefore, reduce the conductivity. It is also worth noting that the real Fermi arcs have nontrivial spin polarization [1, 29, 52]. This feature is left out in our model. Whether the spin texture of Fermi arc states is relevant for the Fermi arc transport is probably a material dependent property. In this connection, we would like to note that, according to the recent experimental results in Ref. [34], the spin texture does play a qualitative, although minor, role in TaAs. We assumed also that impurities are dilute so that our perturbative treatment of the self-energy and the current-current correlator is justified. In the regime of strong disorder, one should use a self-consistent Born approximation, renormalization group, or other non-perturbative techniques. In addition, the localization effects should be taken into account at large disorder strength.

### Acknowledgments

The work of E.V.G. was supported partially by the Ukrainian State Foundation for Fundamental Research. The work of V.A.M. was supported by the Natural Sciences and Engineering Research Council of Canada. The work of I.A.S. was supported in part by the U.S. National Science Foundation under Grant No. PHY-1404232.

- 
- [1] Z. Wang, Y. Sun, X. Q. Chen, C. Franchini, G. Xu, H. Weng, X. Dai, and Z. Fang, *Phys. Rev. B* **85**, 195320 (2012).
  - [2] Z. Wang, H. Weng, Q. Wu, X. Dai, and Z. Fang, *Phys. Rev. B* **88**, 125427 (2013).
  - [3] S. Borisenko, Q. Gibson, D. Evtushinsky, V. Zabolotnyy, B. Buchner, and R. J. Cava, *Phys. Rev. Lett.* **113**, 027603 (2014).
  - [4] M. Neupane, S.-Y. Xu, R. Sankar, N. Alidoust, G. Bian, C. Liu, I. Belopolski, T.-R. Chang, H.-T. Jeng, H. Lin, A. Bansil, F. Chou, and M. Z. Hasan, *Nature Commun.* **5**, 3786 (2014).
  - [5] Z. K. Liu, B. Zhou, Y. Zhang, Z. J. Wang, H. M. Weng, D. Prabhakaran, S.-K. Mo, Z. X. Shen, Z. Fang, X. Dai, Z. Hussain, and Y. L. Chen, *Science* **343**, 864 (2014).
  - [6] X. Wan, A. M. Turner, A. Vishwanath, and S. Y. Savrasov, *Phys. Rev. B* **83**, 205101 (2011).
  - [7] C. Zhang, Z. Yuan, S. Xu, Z. Lin, B. Tong, M. Z. Hasan, J. Wang, C. Zhang, and S. Jia, arXiv:1502.00251.
  - [8] S.-Y. Xu, I. Belopolski, N. Alidoust, M. Neupane, C. Zhang, R. Sankar, S.-M. Huang, C.-C. Lee, G. Chang, B. Wang, G. Bian, H. Zheng, D. S. Sanchez, F. Chou, H. Lin, S. Jia, and M. Z. Hasan, *Science* **349**, 613, (2015).
  - [9] B. Q. Lv, H. M. Weng, B. B. Fu, X. P. Wang, H. Miao, J. Ma, P. Richard, X. C. Huang, L. X. Zhao, G. F. Chen, Z. Fang, X. Dai, T. Qian, and H. Ding, *Phys. Rev. X* **5**, 031013 (2015).
  - [10] X. Huang, L. Zhao, Y. Long, P. Wang, D. Chen, Z. Yang, H. Liang, M. Xue, H. Weng, Z. Fang, X. Dai, and G. Chen, *Phys. Rev. X* **5**, 031023 (2015).
  - [11] I. Belopolski, S.-Y. Xu, Y. Ishida, X. Pan, P. Yu, D. S. Sanchez, M. Neupane, N. Alidoust, G. Chang, T.-R. Chang, Y. Wu, G. Bian, H. Zheng, S.-M. Huang, C.-C. Lee, D. Mou, L. Huang, Y. Song, B. Wang, G. Wang, Y.-W. Yeh, N. Yao, J. Rault, P. Lefevre, F. Bertran, H.-T. Jeng, T. Kondo, A. Kaminski, H. Lin, Z. Liu, F. Song, S. Shin, and M. Z. Hasan, arXiv:1512.09099.
  - [12] S. Borisenko, D. Evtushinsky, Q. Gibson, A. Yaresko, T. Kim, M. N. Ali, B. Buechner, M. Hoesch, and R. J. Cava, arXiv:1507.04847.
  - [13] S. L. Adler, *Phys. Rev.* **177**, 2426 (1969); J. S. Bell and R. Jackiw, *Nuovo Cim. A* **60**, 47 (1969).
  - [14] D. E. Kharzeev, J. Liao, S. A. Voloshin, and G. Wang, arXiv:1511.04050.
  - [15] H. B. Nielsen and M. Ninomiya, *Phys. Lett. B* **130**, 389 (1983).
  - [16] H.-J. Kim, K.-S. Kim, J. F. Wang, M. Sasaki, N. Satoh, A. Ohnishi, M. Kitaura, M. Yang, and L. Li, *Phys. Rev. Lett.* **111**, 246603 (2013).
  - [17] D. T. Son and B. Z. Spivak, *Phys. Rev. B* **88**, 104412 (2013).
  - [18] E. V. Gorbar, V. A. Miransky, and I. A. Shovkovy, *Phys. Rev. B* **89**, 085126 (2014).
  - [19] P. Goswami, J. H. Pixley, and S. Das Sarma, *Phys. Rev. B* **92**, 075205 (2015).
  - [20] K. von Klitzing, G. Dorda, and M. Pepper, *Phys. Rev. Lett.* **45**, 494 (1980).
  - [21] D. J. Thouless, M. Kohmoto, M. P. Nightingale, and M. den Nijs, *Phys. Rev. Lett.* **49**, 405 (1982).
  - [22] F. D. M. Haldane, *Phys. Rev. Lett.* **61**, 2015 (1988).

- [23] M. König, S. Wiedmann, C. Brune, A. Roth, H. Buhmann, L. Molenkamp, X.-L. Qi, and S.-C. Zhang, *Science* **318**, 766 (2007).
- [24] C. L. Kane and E. J. Mele, *Phys. Rev. Lett.* **95**, 146802 (2005).
- [25] V. Aji, *Phys. Rev. B* **85**, 241101 (2012).
- [26] F. D. M. Haldane, arXiv:1401.0529.
- [27] R. M. Feenstra, J. A. Stroscio, and A. P. Fein, *Surf. Sci.* **181**, 295 (1987).
- [28] M. F. Crommie, C. P. Lutz, and D. M. Eigler, *Nature* **363**, 524 (1993).
- [29] G. Chang, S.-Y. Xu, H. Zheng, C.-C. Lee, S.-M. Huang, I. Belopolski, D. S. Sanchez, G. Bian, N. Alidoust, T.-R. Chang, C.-H. Hsu, H.-T. Jeng, A. Bansil, H. Lin, and M. Z. Hasan, *Phys. Rev. Lett.* **116**, 066601 (2016).
- [30] S. Kourtis, J. Li, Z. Wang, A. Yazdani, and B. A. Bernevig, *Phys. Rev. B* **93**, 041109(R) (2016).
- [31] A. K. Mitchell and L. Fritz, *Phys. Rev. B* **93**, 035137 (2016).
- [32] H. Zheng, S.-Y. Xu, G. Bian, C. Guo, G. Chang, D. S. Sanchez, I. Belopolski, C.-C. Lee, S.-M. Huang, X. Zhang, R. Sankar, N. Alidoust, T.-R. Chang, F. Wu, T. Neupert, F. Chou, H.-T. Jeng, N. Yao, A. Bansil, S. Jia, H. Lin, and M. Z. Hasan, *ACS Nano*, **10** (1), 13781385 (2016).
- [33] R. Batabyal, N. Morali, N. Avraham, Y. Sun, M. Schmidt, C. Felser, A. Stern, B. Yan, and H. Beidenkopf, arXiv:1603.00283.
- [34] H. Inoue, A. Gyenis, Z. Wang, J. Li, S. W. Oh, S. Jiang, N. Ni, B. A. Bernevig, and A. Yazdani, *Science* **351**, 1184 (2016).
- [35] P. Hosur, *Phys. Rev. B* **86**, 195102 (2012).
- [36] E. V. Gorbar, V. A. Miransky, I. A. Shovkovy, and P. O. Sukhachov, *Phys. Rev. B* **91**, 121101 (2015).
- [37] A. C. Potter, I. Kimchi, and A. Vishwanath, *Nature Commun.* **5**, 5161 (2014).
- [38] Y. Baum, E. Berg, S. A. Parameswaran, and A. Stern, arXiv:1508.03047.
- [39] P. J. W. Moll, N. L. Nair, T. Helm, A. C. Potter, I. Kimchi, A. Vishwanath, and J. G. Analytis, arXiv:1505.02817.
- [40] E. V. Gorbar, V. A. Miransky, I. A. Shovkovy, and P. O. Sukhachov, *Phys. Rev. B* **90**, 115131 (2014).
- [41] D. Bulmash and X.-L. Qi, arXiv:1512.03437.
- [42] P. G. Derry, A. K. Mitchell, and D. E. Logan, *Phys. Rev. B* **92**, 035126 (2015).
- [43] R. Okugawa and S. Murakami, *Phys. Rev. B* **89**, 235315 (2014).
- [44] S.-Q. Shen, *Topological Insulators: Dirac Equation in Condensed Matters* (Springer, 2013).
- [45] R. E. Prange and S. M. Girvin, *The Quantum Hall effect* (Springer-Verlag, 1990).
- [46] M. Abramowitz and I. A. Stegun, *Handbook of mathematical functions: with formulas, graphs, and mathematical tables* (Dover Publications, 1964).
- [47] L. S. Levitov and A. V. Shytov, *The Green's functions. Problems with solutions* (Fizmatlit, 2002).
- [48] I. M. Lifshitz, *Sov. Phys. JETP* **11**, 1130 (1960).
- [49] S.-Y. Xu, C. Liu, I. Belopolski, S. K. Kushwaha, R. Sankar, J. W. Krizan, T.-R. Chang, C. M. Polley, J. Adell, T. Balasubramanian, K. Miyamoto, N. Alidoust, G. Bian, M. Neupane, H.-T. Jeng, C.-Y. Huang, W.-F. Tsai, T. Okuda, A. Bansil, F. C. Chou, R. J. Cava, H. Lin, and M. Z. Hasan, *Phys. Rev. B* **92**, 075115 (2015).
- [50] R. Nandkishore, D. A. Huse, and S. L. Sondhi, *Phys. Rev. B* **89**, 245110 (2014).
- [51] Ya. I. Rodionov and S. V. Syzranov, *Phys. Rev. B* **91**, 195107 (2015).
- [52] S.-Y. Xu, I. Belopolski, D. S. Sanchez, M. Neupane, G. Chang, K. Yaji, Z. Yuan, C. Zhang, K. Kuroda, G. Bian, C. Guo, H. Lu, T.-R. Chang, N. Alidoust, H. Zheng, C.-C. Lee, S.-M. Huang, C.-H. Hsu, H.-T. Jeng, A. Bansil, A. Alexandradinata, T. Neupert, T. Kondo, F. Komori, S. Shin, H. Lin, S. Jia, and M. Z. Hasan, arXiv:1510.08430.